1   **PDGFRα/β heterodimer activation negatively affects downstream ERK1/2 signaling and cellular**

2   **proliferation**

3

4   Maria B. Campaña[1], Madison R. Perkins[1], Maxwell C. McCabe[2], Andrew Neumann[1], Eric D.

5   Larson[3], Katherine A. Fantauzzo[1*]

6

7   [1]Department of Craniofacial Biology, School of Dental Medicine, University of Colorado

8   Anschutz Medical Campus, Aurora, CO 80045, USA

9   [2]Department of Biochemistry and Molecular Genetics, School of Medicine, University of

10   Colorado Anschutz Medical Campus, Aurora, CO 80045, USA

11   [3]Department of Basic and Translational Sciences, School of Dental Medicine, University of

12   Pennsylvania, Philadelphia, PA 19104, USA

13   [*]Corresponding author. Email: katherine.fantauzzo@cuanschutz.edu

One-sentence summary

PDGFRα/β heterodimer binding to MYO1D contributes to rapid internalization of the dimerized receptors, thereby negatively affecting downstream ERK1/2 signaling and cellular proliferation.

Abstract

The platelet-derived growth factor receptor (PDGFR) family of receptor tyrosine kinases allows cells to communicate with one another by binding to growth factors at the plasma membrane and activating intracellular signaling pathways to elicit responses such as migration, proliferation, survival and differentiation. The PDGFR family consists of two receptors, PDGFRα and PDGFRβ, that dimerize to form PDGFRα homodimers, PDGFRα/β heterodimers and PDGFRβ homodimers. Here, we overcame prior technical limitations in visualizing and purifying PDGFRα/β heterodimers by generating a cell line stably expressing C-terminal fusions of PDGFRα and PDGFRβ with bimolecular fluorescence complementation fragments corresponding to the N-terminal and C-terminal regions of the Venus fluorescent protein, respectively. We found that these receptors heterodimerize relatively quickly in response to PDGF-BB ligand treatment, with a peak of receptor autophosphorylation following 5 minutes of ligand stimulation. Moreover, we demonstrated that PDGFRα/β heterodimers are rapidly internalized into early endosomes, particularly signaling endosomes, where they dwell for extended lengths of time. We showed that PDGFRα/β heterodimer activation does not induce downstream phosphorylation of ERK1/2 and significantly inhibits cell proliferation. Further, we characterized the PDGFR dimer-specific interactome and identified MYO1D as a novel protein that preferentially binds PDGFRα/β heterodimers. We demonstrated that knockdown of MYO1D leads to retention of PDGFRα/β heterodimers at the plasma membrane, resulting in increased

2

37 phosphorylation of ERK1/2 and increased cell proliferation. Collectively, our findings impart

38 valuable insight into the molecular mechanisms by which specificity is introduced downstream

39 of PDGFR activation to differentially propagate signaling and generate distinct cellular

40 responses.

41

42 **INTRODUCTION**

43   The platelet-derived growth factor receptor (PDGFR) family of receptor tyrosine kinases

44 (RTKs) allows cells to communicate with one another by binding to growth factors at the plasma

45 membrane and activating intracellular signaling pathways to elicit responses such as migration,

46 proliferation, survival and differentiation (*1, 2*). The mammalian PDGF family is composed of

47 four dimeric ligands, PDGF-AA, PDGF-BB, PDGF-CC and PDGF-DD, which variously signal

48 through two receptors, PDGFRα and PDGFRβ. These receptors possess an extracellular ligand-

49 binding domain harboring five immunoglobulin-like loops, a single transmembrane domain and

50 an intracellular domain containing a split, catalytic tyrosine kinase (*3*). PDGFRα and PDGFRβ

51 share the highest amino acid homology in the kinase domains, with significantly reduced

52 homology in the extracellular and interkinase domains (*4*). Upon ligand binding, the PDGFRs

53 dimerize to form PDGFRα homodimers, PDGFRα/β heterodimers or PDGFRβ homodimers (*4-*

54 *8*). Through an undetermined mechanism, dimerization subsequently promotes tyrosine kinase

55 activity, resulting in the trans-autophosphorylation of intracellular tyrosine residues (*6, 9*).

56 Signaling molecules and adaptor proteins containing Src homology 2 phosphotyrosine

57 recognition motifs subsequently bind to specific phosphorylated residues in the receptors to

58 initiate downstream intracellular signaling cascades (*1, 3*).

3

59   Based on *in vivo* mouse knockout phenotypes, the ligands PDGF-AA and PDGF-CC have

60   been shown to solely activate PDGFRα signaling during development, while PDGF-BB

61   activates PDGFRβ signaling (*10-14*). Alternatively, the ligand PDGF-DD is not essential for

62   development nor postnatal life (*15*). While this data is often interpreted as representing the

63   functional roles of PDGFRα homodimers and PDGFRβ homodimers, compelling evidence has

64   emerged indicating that PDGFRα/β heterodimers also form during development. First, analysis

65   of autophosphorylation mutant knockin alleles in mice suggested that PDGFRβ is able to

66   compensate for the loss of PI3K signaling through PDGFRα upon heterodimer formation (*16*).

67   Embryos homozygous for an allele (*Pdgfra^{PI3K}*) in which PDGFRα is unable to bind PI3K due to

68   two tyrosine to phenylalanine mutations (*17*) die perinatally and exhibit palatal clefting, among

69   other abnormalities (*8, 16*). However, these embryos do not display the full range of skeletal

70   defects, such as overt facial clefting, observed in *Pdgfra*-null embryos (*11*). In support of

71   PDGFRα/β heterodimer formation, whereas *Pdgfrb^{PI3K/PI3K}* mice do not exhibit craniofacial

72   defects (*18*), *Pdgfra^{PI3K/PI3K};Pdgfrb^{PI3K/PI3K}* double-homozygous mutant embryos in which PI3K

73   signaling cannot be engaged through PDGFRα/β heterodimers phenocopy *Pdgfra*-null embryos

74   (*16*). More recently, we and others have demonstrated that PDGFRα and PDGFRβ genetically

75   and physically interact in the murine embryonic mesenchyme, primarily in response to PDGF-

76   BB ligand (*8, 19-21*). However, definitive proof of the formation of active PDGFRα/β

77   heterodimers has remained elusive.

78   Technical limitations had previously prevented an unbiased analysis of PDGFR dimer-

79   specific dynamics, as antibodies cannot differentiate between receptors present as monomers or

80   engaged in homodimers versus heterodimers. Further, ligand identity alone cannot inform dimer-

81   specific conclusions, as some PDGF ligands, especially PDGF-BB, are promiscuous and can

82   result in the formation of multiple dimers (*8*). To overcome these limitations, we recently

83   developed a novel bimolecular fluorescence complementation (BiFC) (*22, 23*) approach that

84   enabled us to visualize and purify activated PDGFRα homodimers and PDGFRβ homodimers

85   (*24*). We cloned plasmids expressing C-terminal fusions of each PDGFR with BiFC fragments

86   corresponding to the N-terminal (V1) or C-terminal (V2) regions of the Venus fluorescent protein

87   (*23*). The individual N- and C-terminal fragments are non-fluorescent when bound to monomeric

88   receptors. However, upon receptor dimerization, the N- and C-terminal fragments colocalize,

89   resulting in a functional Venus protein that can be visualized by fluorescence microscopy or

90   purified biochemically using a GFP-Trap nanobody that has an epitope spanning V1 and V2

91   (*25*). Using this approach, we demonstrated that PDGFRα receptors homodimerize slowly, have

92   decreased levels of autophosphorylation, are rapidly internalized into early endosomes and are

93   quickly degraded via late endosome trafficking to the lysosome. Alternatively, we found that

94   PDGFRβ receptors homodimerize quickly, have increased levels of autophosphorylation, are

95   slowly internalized and are more likely to be recycled to the plasma membrane via recycling

96   endosomes (*24*). We showed that these dynamics lead to a greater amplitude of ERK1/2 and

97   AKT phosphorylation downstream of PDGFRβ homodimer activation, in addition to increased

98   proliferation and migration (*24*). While these findings provided considerable insight into

99   mechanisms by which specificity is introduced downstream of PDGFR activation, the protein

100   interactions that mediate the internalization and trafficking of the various PDGFR dimers are

101   incompletely understood.

102   Here, we employed the same BiFC approach to examine the dimerization, activation,

103   internalization and trafficking dynamics of PDGFRα/β heterodimers, as well as their effect on

104   intracellular signaling and cellular behavior, revealing significant differences from what we

105 previously observed for the PDGFR homodimers (*24*). Further, we generated the first PDGFR

106 dimer-specific interactome, identifying proteins that differentially bind the three PDGFR dimers

107 and contribute to receptor internalization following activation at the plasma membrane.

108 Combined, these findings substantially expand our understanding of the mechanisms by which

109 the various PDGFR dimers propagate downstream signaling to generate distinct cellular outputs.

110

111 **RESULTS**

112 **Generation and validation of a PDGFRα/β-BiFC stable cell line**

113   To investigate PDGFRα/β-specific dynamics, and compare these to what we previously

114 observed for PDGFRα homodimers and PDGFRβ homodimers (*24*), we stably integrated

115 PDGFRα-V1 and PDGFRβ-V2 sequences (Fig. S1A) into the human-derived HCC15 cell line

116 via lentiviral transduction. We chose this cell line due to its mesenchymal expression profile,

117 lack of *PDGFRA* and *PDGFRB* expression, minimal expression of the various PDGF ligands

118 (with only *PDGFA* being expressed at a low reads per kilobase million (RPKM) value of 2.70),

119 and a spread out morphology that allows for examination of trafficking events (*26, 27*).

120 PDGFRα-V1 and PDGFRβ-V2 sequence integration was confirmed by PCR amplification and

121 Sanger sequencing. Quantitative real-time PCR (qRT-PCR) revealed that the transcripts encoding

122 *PDGFRA* (1.48±0.247% of *B2M* expression; mean±s.e.m.) and *PDGFRB* (1.14±0.365% of *B2M*

123 expression) were expressed at similar levels (Fig. S1B). Lastly, we demonstrated that both

124 PDGFRα and PDGFRβ proteins were expressed in the PDGFRα/β heterodimer cell line and

125 migrated at the expected masses via western blotting (Fig. S1C).

126   To confirm the Venus complementation event upon exogenous ligand treatment, we

127 starved the cells for 24 h in HITES medium lacking any growth factors, photobleached and

6

128   stimulated the cells with PDGF-BB ligand for 5 min. We had previously demonstrated that

129   PDGFRα/β heterodimers form most robustly in response to PDGF-BB ligand treatment of both

130   primary mouse embryonic fibroblasts (MEFs) and mouse embryonic palatal mesenchyme

131   (MEPM) cells (*8, 20*). We observed little to no Venus expression in the absence of ligand

132   treatment (Fig. 1A) and robust Venus expression surrounding the nucleus and at the periphery of

133   the cell following ligand stimulation (Fig. 1B). Quantification of fluorescence intensity

134   demonstrated a significant increase in Venus intensity between no ligand treatment (6.61±0.264

135   arbitrary units (A.U.); mean±s.e.m.) and 5 min of PDGF-BB treatment (34.9±4.51 A.U.) (Fig.

136   1C). We next examined colocalization of the Venus signal with signals from anti-PDGFRα and

137   anti-PDGFRβ antibodies. In each case, Venus signal colocalized with a subset of PDGFR

138   expression (Fig. 1D to F). The extent of colocalization of the Venus signal with signals from anti-

139   PDGFRα (0.346±0.0359 Pearson's correlation coefficient (PCC); mean±s.e.m.) and anti-

140   PDGFRβ (0.359±0.0678 PCC) antibodies was comparable in the PDGFRα/β heterodimer cell

141   line (Fig. 1D). The observed PCC values less than 1 indicated that the presence of the BiFC

142   fragments alone was not driving heterodimerization (Fig. 1D). The regions of receptor

143   expression that were not Venus-positive (Fig. 1E and F) likely represent monomeric receptors

144   and/or potential PDGFRαV1/αV1 and especially PDGFRβV2/βV2 homodimers, which would

145   not be expected to fluoresce.

146

147   **PDGFRα/β heterodimers dimerize relatively quickly and have peak levels of**

148   **autophosphorylation following 5 minutes of ligand treatment**

149   To confirm the Venus complementation event upon exogenous ligand treatment

150   biochemically, we stimulated the cells with PDGF-BB ligand for 2 and 5 min. Lysates were

7

151   immunoprecipitated with the GFP-Trap nanobody and subjected to western blotting for

152   PDGFRα and PDGFRβ, normalizing the immunoprecipitation signal to the whole-cell lysate

153   signal for each receptor. We found that the receptors heterodimerize relatively quickly, with peak

154   dimerization following 5 min of ligand treatment for both PDGFRα (2.17±1.27 relative

155   induction (R.I.); mean±s.e.m.) and PDGFRβ (1.95±0.173 R.I.) (Fig. 2A and B). As would be

156   expected for heterodimers, the relative induction values for the two receptors were essentially

157   equal throughout the time course (Fig. 2B). We next examined activation of the receptors by

158   assessing receptor autophosphorylation. Cells were stimulated with PDGF-BB ligand in a time

159   course from 2 min to 4 h. Whole-cell lysates were immunoprecipitated with the GFP-Trap

160   nanobody and subjected to western blotting with an anti-phospho-PDGFR antibody, which

161   recognizes a phosphorylated tyrosine residue within the tyrosine kinase domains of both

162   PDGFRα and PDGFRβ. Consistent with previous findings demonstrating that both ligand

163   binding and dimerization are required for receptor activation (*9, 24, 28*), we observed minimal

164   phospho-PDGFR signal in the absence of ligand stimulation (Fig. 2C). However, the receptors

165   were significantly autophosphorylated in response to ligand treatment, with peak activation

166   following 5 min of PDGF-BB stimulation (6.61±1.75 R.I.) (Fig. 2C and D). As we previously

167   observed, the anti-PDGFR blots contained two bands representing the non-glycosylated and

168   glycosylated forms of the receptors (*7, 24*), while the anti-phospho-PDGFR blots possessed a

169   single band representing the glycosylated, phosphorylated versions of the receptors upon ligand

170   treatment (*24*).

171

172   **PDGFRα/β heterodimers are rapidly internalized into signaling endosomes**

173   Following dimerization and activation at the cell membrane in response to ligand

174 binding, PDGFRs are internalized and trafficked through the early endosome before being

175 trafficked to the lysosome via late endosomes for degradation or recycled to the membrane via

176 recycling endosomes for continued signaling (*24, 29-33*). To investigate the trafficking dynamics

177 of PDGFRα/β heterodimers in response to ligand treatment, we examined colocalization of the

178 Venus signal in our PDGFRαV1/βV2 cell line with markers of various subcellular

179 compartments. We found that PDGFRα/β heterodimers were rapidly internalized, as indicated by

180 a significant decrease in colocalization with the plasma membrane marker Na^+/K^+-ATPase (*34*)

181 from the 1 min (0.217±0.0134 PCC) to 5 min (0.068±0.00956 PCC) ligand treatment timepoints

182 (Fig. 3A to C). Further, analysis of Venus colocalization with the early endosome marker Rab5

183 (all isoforms) (*35*) demonstrated that PDGFRα/β heterodimers were internalized into early

184 endosomes, where they dwelled at relatively stable levels from 2 min (0.446±0.0401 PCC) to 30

185 min (0.404±0.0503 PCC) following ligand treatment (Fig. 3D to F). PDGFRα/β heterodimers

186 were primarily found in signaling endosomes during this time, as colocalization values were

187 higher for the signaling endosome marker APPL1 (*36*) at 2 min (0.193±0.0468 PCC) and 30 min

188 (0.245±0.0476 PCC) of ligand treatment (Fig. 3G to I) than the non-signaling endosome marker

189 EEA1 (*37*) at these same timepoints (0.0932±0.0116 PCC and 0.0344±0.0136 PCC, respectively)

190 (Fig. S2A to C). Following trafficking to the early endosomes, the PDGFRα/β heterodimers were

191 subsequently trafficked to RAB7-positive late endosomes (all isoforms) (*35*) (Fig. S2D and E),

192 RAB4-positive rapid recycling endosomes (all isoforms) (*35*) (Fig. S2F and G) and RAB11-

193 positive slow recycling endosomes (all isoforms) (*35*) (Fig. S2H and I). Colocalization of Venus

194 signal with Na^+/K^+-ATPase at 60 min (0.199±0.0132 PCC) and 90 min (0.178±0.0115 PCC) of

195 ligand treatment (Fig. S2J and K) was comparable to that following 1 min of ligand treatment

196   described above (Fig. 3A and B), suggesting that a subset of PDGFRα/β heterodimers are

197   recycled following ligand stimulation. Collectively, these data indicate that PDGFRα/β

198   heterodimers are rapidly internalized into signaling endosomes, where they dwell for extended

199   lengths of time, before being trafficked for degradation and recycling.

200

201   **PDGFRα/β heterodimer activation does not induce downstream phosphorylation of**

202   **ERK1/2 and inhibits cell proliferation**

203   To examine the effects of the above PDGFRα/β heterodimer-specific trafficking

204   dynamics on downstream intracellular signaling, we performed a time course of ligand

205   stimulation from 2 min to 4 h followed by western blotting of whole-cell lysates for

206   phosphorylation of two effector molecules downstream of PDGFR activation, ERK1/2 and AKT

207   (all isoforms) (*8, 24, 38*). PDGFRα/β heterodimer activation did not induce downstream

208   phosphorylation of ERK1/2, as relative induction levels did not increase beyond baseline levels

209   at 0 min of ligand stimulation (1.00±0.00 R.I.) until 4 h of PDGF-BB treatment (1.08±0.506 R.I.)

210   (Fig. 4A and B). Alternatively, PDGFRα/β heterodimer activation led to a very transient

211   phospho-AKT response, with a peak at 5 min of ligand stimulation (2.74±0.202 R.I.) and a return

212   to near baseline levels by 30 min of PDGF-BB treatment (1.27±0.366 R.I.) that remained

213   relatively stable throughout the rest of the time course (1.25±0.194 R.I. at 4 h) (Fig. 4C and D).

214   Proliferation is increased downstream of both PDGFRα and PDGFRβ signaling in

215   settings where both receptors are active (*21, 39, 40*). To determine how the above trafficking and

216   signaling dynamics affect cellular activity downstream of PDGFRα/β heterodimer activation, we

217   assessed cell proliferation via a soft agar anchorage-independent growth assay in RPMI growth

218   medium with 10% fetal bovine serum (FBS) over the course of 10 days. As expected, HCC15

219   cells, which do not express PDGFRs, did not have significantly increased colony count nor

220   colony area upon PDGF-BB ligand stimulation (Fig. 4E,G and H). In the absence and presence

221   of PDGF-BB ligand, parental HCC15 cells grew visible colonies by the end of the assay (Fig.

222   4E), with $2.97 \times 10^3 \pm 4.59 \times 10^2$ colonies (mean±s.e.m.) and $5.97 \times 10^3 \pm 8.80 \times 10^2$ colonies (Fig. 4G),

223   and $4.14 \times 10^5 \pm 7.21 \times 10^4$ A.U. and $3.29 \times 10^5 \pm 2.96 \times 10^4$ A.U. total colony area (Fig. 4H),

224   respectively. PDGFRαV1/βV2 cells, however, proliferated less than parental HCC15 cells, and

225   significantly so in the presence of PDGF-BB ligand (Fig. 4F), with $1.04 \times 10^3 \pm 1.64 \times 10^2$ colonies

226   (Fig. 4G) and $1.38 \times 10^4 \pm 7.52 \times 10^3$ A.U. total colony area (Fig. 4H).

227   Given that PDGFRβ homodimers and PDGFRα/β heterodimers bind the same ligand,

228   PDGF-BB, together, these findings indicated that PDGFRα/β heterodimers may serve as sinks

229   that bind PDGF-BB and prevent the ligand from activating PDGFRβ homodimers. To test this

230   hypothesis, we first demonstrated that PDGF-BB ligand could activate PDGFRβ homodimers in

231   our PDGFRαV1/βV2 cell line. We stimulated PDGFRαV1/βV2 cells with PDGF-BB ligand,

232   resulting in the potential formation of both PDGFRα/β heterodimers and PDGFRβ homodimers.

233   Following immunoprecipitation with the GFP-Trap nanobody, which should only pull down

234   PDGFRα/β heterodimers, the supernatant was immunoprecipitated with an anti-PDGFRβ

235   antibody, which should isolate PDGFRβ monomers and PDGFRβ homodimers. Each sample

236   was then subjected to western blotting with the anti-phospho-PDGFR antibody to identify

237   activated dimers (Fig. S3A). This experiment revealed that both active PDGFRα/β heterodimers

238   and PDGFRβ homodimers formed (Fig. S3B). However, there was only a 4.41±1.56 R.I. for

239   PDGFRβ homodimers following 5 min of ligand stimulation in the PDGFRαV1/βV2 cell line

240   (Fig. S3C), compared to a 26.8±2.04 R.I. that we previously observed at this same timepoint in

241   the PDGFRβV1/βV2 cell line (*24*), indicating that PDGFRα/β heterodimers may indeed serve as

242   ligand sinks.

243

244   **MYO1D preferentially binds PDGFRα/β heterodimers**

245   We next combined BiFC with stable isotope labeling by amino acids in cell culture

246   (SILAC) and quantitative mass spectrometry to identify proteins that differentially interact with

247   the various PDGFR dimers at the time of internalization. We used a control cell line with

248   myristoylated, membrane-targeted Venus, as well as our PDGFRαV1/αV2 (*24*),

249   PDGFRαV1/βV2 and PDGFRβV1/βV2 (*24*) cell lines representing each of the three PDGFR

250   dimers. Cells were either grown in the presence of medium with light isotopes and left

251   unstimulated, or grown in the presence of medium with heavy isotopes and stimulated with the

252   relevant PDGF ligand for 5 minutes. Following cell lysis and extraction, we mixed light and

253   heavy samples 1:1 for each cell line, immunoprecipitated the receptor dimers and interacting

254   proteins with the GFP-Trap nanobody, and generated tryptic peptides for mass spectrometry

255   analysis (Fig. 5A). Following total signal normalization and removal of common contaminants

256   (*41*) that were not differentially detected across samples, we filtered the proteins based on three

257   criteria to identify those with increased binding to one or more PDGFR dimer in response to

258   PDGF ligand treatment: 1) the protein had to be present in both mass spectrometry biological

259   replicates for a given cell line, 2) the heavy/light ratio for the experimental sample had to be

260   greater than that for the control myristoylated Venus sample, and 3) the experimental sample

261   heavy/light ratio had to be greater than 1. These parameters generated a list of 350 total proteins,

262   with 177 proteins binding PDGFRα homodimers, and 199 and 217 proteins binding PDGFRα/β

263   heterodimers and PDGFRβ homodimers, respectively. Of these, 71 proteins were shared amongst

264 all three PDGFR dimers, 51 were unique to PDGFRα homodimers, 67 were unique to

265 PDGFRα/β heterodimers, and 60 were unique to PDGFRβ homodimers (Fig. 5B).

266 Known PDGFR-binding proteins were detected in our mass spectrometry screen. For

267 example, the catalytic subunit of PI3K, p110β, was bound to both PDGFRα/β heterodimers and

268 PDGFRβ homodimers, however only in a single biological replicate for each dimer. Gene

269 ontology (GO) analysis with the Enrichr tool (*42*) demonstrated that the most enriched biological

270 process annotations for the 71 proteins common to all three dimers related to mRNA processing

271 and mRNA splicing, as well as anterograde dendritic transport (Fig. S4). The proteins unique to

272 PDGFRα homodimers were additionally enriched for terms related to cytoskeleton organization,

273 regulation of DNA recombination, mitosis, regulation of protein localization to the nucleus and

274 regulation of p53 signal transduction (Fig. S4). The proteins unique to PDGFRα/β heterodimers

275 were additionally enriched for nucleosome assembly and organization, regulation of autophagy,

276 regulation of immunoglobulin production and regulation of gene expression (Fig. S4). Finally,

277 the proteins unique to PDGFRβ homodimers were additionally enriched for retrograde vesicle-

278 mediated transport, regulation of ubiquitin-protein transferase activity, nucleosome disassembly

279 and regulation of microtubule depolymerization and nucleation (Fig. S4), possibly pointing to

280 unique functions for the individual dimers.

281 Given our demonstration that the various PDGFR dimers have different trafficking

282 dynamics (*24*), we next performed GO analysis of our filtered proteins to identify those involved

283 in trafficking that differentially interact with the various PDGFR dimers (Fig. 5C). While some

284 of these 20 proteins had been implicated in RTK binding, none had previously been reported to

285 interact with the PDGFRs. We chose to focus our initial studies on unconventional myosin-Id

286 (MYO1D), as this protein was not detected in the control myristoylated Venus sample and had

287   differential interaction with the various PDGFR dimers upon ligand stimulation, with the greatest

288   binding to PDGFRα/β heterodimers (Fig. 5C). Further, MYO1D had previously been shown to

289   bind and affect the subcellular localization of the RTKs EGFR, ERBB2 and ERBB4 (*43*). We

290   confirmed that MYO1D preferentially binds PDGFRα/β heterodimers via immunoprecipitation

291   of whole-cell lysates from each cell line with the GFP-Trap nanobody followed by western

292   blotting with an anti-MYO1D antibody (Fig. 5D). Further, these results confirmed our mass

293   spectrometry results that MYO1D exhibits increased binding to PDGFRα/β heterodimers upon 5

294   min of PDGF-BB ligand treatment compared to binding levels in unstimulated cells (Fig. 5D).

295   Of note, we observed increased MYO1D expression in whole-cell lysates from the

296   PDGFRαV1/βV2 cell line compared to both the PDGFRαV1/αV2 homodimer and

297   PDGFRβV1/βV2 homodimer cell lines (Fig. 5D). Quantitative RT-PCR indicated that this

298   upregulation is observed on the transcript level as well (Fig. S5). This upregulation could stem

299   from a mutation in the clone chosen for the PDGFRαV1/βV2 cell line, disruption of *MYO1D*

300   regulatory elements upon insertion of the PDGFR-BiFC sequences, and/or increased *MYO1D*

301   transcriptional activity or transcript stability upon PDGFRα/β heterodimer activation. In favor of

302   the latter hypotheses, *MYO1D* expression increased with passage number for the

303   PDGFRαV1/βV2 cell line (Fig. S5). Finally, we examined colocalization of MYO1D with the

304   various PDGFR dimers following 5 min of PDGF ligand stimulation via immunofluorescence

305   analysis, demonstrating significantly increased colocalization with PDGFRα/β heterodimers

306   (0.546 ± 0.0424 PCC) (Fig. 5E) compared to either PDGFRα homodimers (0.113 ± 0.0216 PCC) or

307   PDGFRβ homodimers (0.115 ± 0.0183 PCC) (Fig. 5F).

308

309 **Knockdown of MYO1D leads to retention of PDGFRα/β heterodimers at the plasma**

310 **membrane, increased downstream phosphorylation of ERK1/2 and increased cell**

311 **proliferation**

312   To examine the effects of MYO1D knockdown on PDGFRα/β heterodimer trafficking,

313 we transfected PDGFRαV1/βV2 cells with a Silencer Select negative control siRNA or a

314 combination of two Silencer Select siRNAs targeting *MYO1D* for 48 h. We confirmed efficient

315 knockdown of MYO1D with the siRNAs targeting *MYO1D* via western blotting of whole-cell

316 lysates at this timepoint (Fig. S6). We first assessed colocalization of the Venus signal with

317 Na$^+$/K$^+$-ATPase, demonstrating a significant increase in colocalization upon treatment with

318 siRNAs targeting *MYO1D* (0.164±0.0227 PCC) compared to the negative control

319 (0.0728±0.00644 PCC) following 5 min of ligand stimulation (Fig. 6A to C). Accordingly, we

320 observed a significant decrease in colocalization with RAB5 upon treatment with siRNAs

321 targeting *MYO1D* (0.123±0.0247 PCC) compared to the negative control (0.315±0.0107 PCC) at

322 2 min of ligand stimulation (Fig. 6D to F). We did not detect significant differences in

323 colocalization with RAB7 between the two treatments at 1 h of ligand stimulation (Fig. 6G to I),

324 indicating that knockdown of MYO1D primarily effects early internalization and trafficking

325 dynamics of the PDGFRα/β heterodimers.

326   Further, knockdown of MYO1D lead to changes in intracellular signaling downstream of

327 PDGFRα/β heterodimer activation. Specifically, phospho-ERK1/2 levels were increased upon

328 treatment with siRNAs targeting *MYO1D* at all timepoints tested from 2 min to 4 h, with the

329 largest difference between negative control (1.15±0.234 R.I.) and experimental siRNA treatment

330 (1.51±0.257 R.I.) occurring at 5 min of ligand treatment (Fig. 7A to C). Alternatively, phospho-

331 AKT levels were decreased upon treatment with siRNAs targeting *MYO1D* at the majority of

332   timepoints tested, with the largest difference between negative control (1.90±0.276 R.I.) and

333   experimental siRNA treatment (1.67±0.0927 R.I.) also occurring at 5 min of ligand treatment

334   (Fig. 7D to F).

335   Finally, we assessed cell proliferation downstream of PDGFRα/β heterodimer activation

336   upon knockdown of MYO1D. Soft agar anchorage-independent growth assays revealed that

337   PDGFRαV1/βV2 cells treated with negative control (Fig. 7G) proliferated less than the same

338   cells treated with siRNAs targeting *MYO1D* (Fig. 7H) in the absence ($6.07 \times 10^3 \pm 4.00 \times 10^2$ versus

339    $8.03 \times 10^3 \pm 4.22 \times 10^2$ colonies, respectively) and presence ($4.50 \times 10^3 \pm 2.32 \times 10^2$ versus

340    $7.50 \times 10^3 \pm 2.21 \times 10^2$ colonies, respectively) of PDGF-BB ligand (Fig. 7I and J), and significantly

341   so as assessed by colony count (Fig. 7I). Taken together, these data demonstrate that knockdown

342   of MYO1D leads to retention of PDGFRα/β heterodimers at the plasma membrane, further

343   resulting in increased downstream phosphorylation of ERK1/2 and increased cell proliferation.

344

345   **DISCUSSION**

346   In this study, we used the BiFC technique to visualize and purify PDGFRα/β

347   heterodimers, demonstrating that this continues to be an invaluable approach for studying RTK

348   dimer-specific properties (*24, 25, 44*). It is useful to compare our findings across the three

349   PDGFR-BiFC cell lines, as the experimental parameters were identical. First, all three dimers

350   exhibited peak dimerization following 5 min of ligand stimulation, with PDGFRα/β

351   heterodimers exhibiting an intermediate speed of dimerization compared to the two homodimers

352   (*24*). Further, the PDGFRα/β heterodimers had considerably reduced levels of

353   autophosphorylation compared to either homodimer, particularly at early ligand stimulation

354   timepoints (*24*). Next, PDGFRα/β heterodimers were internalized into early endosomes more

16

355   quickly and dwelled at that location for longer periods of time than either homodimer (*24*).

356   However, the extent of colocalization of the Venus signal from PDGFRα/β heterodimers and

357   PDGFRβ homodimers with markers of late and recycling endosomes was comparable, indicating

358   that these two dimers undergo degradation and recycling with similar dynamics and are less

359   likely to be degraded and more likely to be recycled than PDGFRα homodimers (*24*). Perhaps

360   most surprisingly, phospho-ERK1/2 levels were not sustained in response to PDGFRα/β

361   heterodimer activation, and the phospho-AKT response, while reaching a higher relative

362   induction than upon PDGFRα homodimer activation, was very transient in the PDGFRα/β

363   heterodimer cell line upon PDGF-BB ligand treatment (*24*). Accordingly, PDGFRα/β

364   heterodimer activation did not induce a proliferative response, unlike the robust proliferation

365   observed upon PDGFRα and PDGFRβ homodimer activation (*24*).

366   One limitation of this study is that we cannot rule out that differences in expression levels

367   of the PDGFRs across our three PDGFR-BiFC cell lines contribute to the disparities in results

368   discussed above. Though we were able to identify a PDGFRα/β heterodimer clone with

369   relatively equal expression of *PDGFRA* and *PDGFRB* among the hundreds of clones screened,

370   the clone had reduced overall levels of these transcripts compared to our PDGFRα homodimer

371   and PDGFRβ homodimer clones (*24*). In the future, it will be critical to compare the dynamics of

372   the various PDGFRs at endogenous expression levels, ideally in a cell type in which there is

373   evidence that all three dimers form, such as the craniofacial mesenchyme (*8*). In that setting,

374   BiFC should continue to serve as a robust approach to both visualize and purify the individual

375   PDGFR dimers. A second limitation of our work is that we cannot be sure that PDGFRα/β

376   heterodimers that colocalize with Na^+/K^+-ATPase at 60 and 90 min of ligand treatment have been

377   recycled. Live-cell imaging over such long timepoints is not possible in our system due to

17

378   photobleaching of Venus. However, the combination of more photostable fluorescent proteins

379   with the BiFC technique should prove a powerful approach to overcome this limitation in the

380   future.

381   Our colocalization studies demonstrated that PDGFRα/β heterodimers are rapidly

382   internalized into the signaling endosome subpopulation of early endosomes, where they dwell for

383   extended lengths of time. The fact that PDGFRα/β heterodimers are not long-lived at the plasma

384   membrane indicates that they are unlikely to generate a robust signaling response at this

385   subcellular platform. Given that the signaling endosome marker APPL1 (*36*) has previously been

386   shown to associate with the RTKs EGFR and TrkA and is required for Akt and Erk1/2 signaling

387   downstream of these receptors (*45-48*), it was unexpected that PDGFRα/β heterodimers did not

388   induce robust and sustained phospho-ERK1/2 and phospho-AKT signals from this site either. It

389   is possible, however, that PDGFRα/β heterodimers may sequester APPL1, thereby preventing it

390   from propagating signaling downstream of other RTKs. In fact, our results point to a similar role

391   for PDGFRα/β heterodimers in serving as sinks that prevent PDGF-BB ligand from binding and

392   activating PDGFRβ homodimers. While the biological significance of this potential function of

393   PDGFRα/β heterodimers is unknown, it is tempting to speculate that heterodimer formation may

394   serve to attenuate PDGFR signaling in instances of cell crowding and/or increased PDGF-BB

395   ligand availability. Though assays comparing the binding affinity of PDGFRα/β heterodimers

396   and PDGFRβ homodimers to PDGF-BB ligand are beyond the scope of this work, such studies

397   would likely shed further light on the role of PDGFRα/β heterodimers.

398   Our mass spectrometry findings represent the first PDGFR dimer-specific interactome

399   and will be a rich resource for the field. Of note, our screen revealed an enrichment for proteins

400   that function in mRNA processing, and specifically mRNA splicing, in binding all three PDGFR

18

401   dimers. PI3K has been identified as the main downstream effector of PDGFRα signaling during

402   murine craniofacial development (*16, 49*). Interestingly, we had previously demonstrated in the

403   context of the facial mesenchyme that phosphorylation targets of Akt downstream of PI3K-

404   mediated PDGFRα homodimer signaling are similarly enriched for proteins involved in RNA

405   processing (*49*) and further, that alternative RNA splicing is the predominant mechanism of gene

406   expression regulation downstream of this signaling pathway (*50*). Taken together, these results

407   indicate that proteins that function in mRNA processing engage with PDGFR signaling on

408   multiple levels: through binding to the receptors and via phosphorylation by downstream

409   effector(s). Moreover, our finding that PDGFRα homodimers interact with proteins that function

410   in organization of the actomyosin cytoskeleton is in line with prior work demonstrating that

411   PDGFRα homodimer signaling drives association of the transcription factor serum response

412   factor (SRF) with the myocardin-related transcription factor-A (MRTFA) cofactor to upregulate

413   expression of gene products that function within the actomyosin cytoskeleton (*51*). Finally, the

414   fact that PDGFRα homodimers bound proteins that function in the regulation of signal

415   transduction by p53 is consistent with our prior finding that PI3K-mediated PDGFRα

416   homodimer signaling regulates p53-dependent intracellular pathways in the context of skeletal

417   development (*49*). Though the full scope of PDGFRα/β heterodimer function remains to be

418   determined, our mass spectrometry results suggest that activation of this dimer may ultimately

419   contribute to nucleosome assembly and organization, and regulation of autophagy,

420   immunoglobulin production and gene expression. Given our findings that PDGFR dimers are

421   dynamically trafficked throughout the cell for several hours following ligand treatment (*24*),

422   similar approaches coupling biochemical purification of the dimers followed by mass

423   spectrometry at multiple timepoints following ligand stimulation should provide a more

424 complete understanding of the PDGFR dimer-specific interactome in various subcellular

425 compartments. Further, as varying concentrations of PDGF ligand have been shown to result in

426 differences in the timing and extent of PDGFR internalization, phosphorylation of downstream

427 effector molecules, proliferation and migration (*52*), analogous experiments to the ones

428 performed here with varying PDGF ligand concentrations should determine whether differential

429 engagement of interacting proteins contributes to these responses.

430 In this study, we identified MYO1D as a novel protein interacting with the PDGFRs and

431 demonstrated that it preferentially binds to dimerized, phosphorylated PDGFRα/β heterodimers.

432 We do not know at this time whether MYO1D binds PDGFRα and/or PDGFRβ in the

433 heterodimer complex, nor at what site(s) in the receptor(s) this binding occurs. These questions

434 will be the subject of future research. However, given that the heavy/light ratio in our mass

435 spectrometry screen was also greater than 1 for the PDGFRα homodimers (1.73), we speculate

436 that MYO1D binds the PDGFRα receptor within the heterodimer complex upon ligand

437 treatment. We found that MYO1D contributes to the rapid internalization of PDGFRα/β

438 heterodimers from the plasma membrane into early endosomes in HCC15 lung cancer cells.

439 Interestingly, these results are in direct contrast to what has previously been demonstrated for

440 EGFR, ERBB2 and ERBB4 in Caco2 colorectal cancer cells. For these members of the ERBB

441 family, MYO1D was shown to bind the unphosphorylated receptors and anchor them in the

442 plasma membrane (*43*). As such, siRNA-mediated knockdown of MYO1D resulted in decreased

443 EGFR, ERBB2 and ERBB4 levels at the plasma membrane (*43*). It is possible that these

444 discrepancies arise due to differing cellular contexts and/or expression levels of the various

445 RTKs in their respective settings. Alternatively, these results may reflect opposing roles for

446   MYO1D in regulating RTK localization and represent a means of divergence across RTK

447   families.

448   Here, we demonstrated that PDGFRα/β heterodimers are rapidly internalized from the

449   plasma membrane into early endosomes, resulting in an absence of phospho-ERK1/2 induction

450   and a transient phospho-AKT response. Alternatively, retention of PDGFRα/β heterodimers at

451   the plasma membrane via knockdown of MYO1D led to increased phospho-ERK1/2 levels and

452   decreased phospho-AKT levels across multiple timepoints of ligand treatment, with the largest

453   differences between negative control and experimental siRNA treatments observed at the

454   relatively early timepoint of 5 min of ligand treatment. These findings indicate that ERK1/2 and

455   AKT phosphorylation downstream of PDGFRα/β activation may primarily occur at the plasma

456   membrane and the early endosome, respectively, immediately following ligand stimulation.

457   Relatedly, our previous results demonstrated that inhibition of clathrin-mediated endocytosis of

458   PDGFRβ homodimers via Dyngo-4a treatment resulted in increased phospho-ERK1/2 levels and

459   decreased phospho-AKT levels at early timepoints of ligand stimulation (*24*), indicating that

460   engagement of these signaling molecules occurs at the same subcellular platforms for

461   PDGFRα/β heterodimers and PDGFRβ homodimers. Alternatively, we previously observed that

462   Dyngo-4a treatment of the PDGFRα homodimer cell line had a negative effect on ERK1/2 and

463   AKT phosphorylation, resulting in delayed and reduced peaks of activation (*24*). These results

464   demonstrated that rapid internalization of PDGFRα homodimers plays an important role in the

465   propagation of downstream signaling and suggested that this dimer primarily signals from early

466   endosomes. Taken together, our findings support a model in which protein interactions and

467   subcellular localization represent mechanisms by which specificity is introduced downstream of

468   PDGFR activation to differentially propagate signaling and generate distinct cellular responses.

469

MATERIALS AND METHODS

Generation of the PDGFRα/β-BiFC-HCC15 and myr-Venus-HCC15 cell lines

The PDGFRαV1/αV2 homodimer and PDGFRβV1/βV2 homodimer cell lines were generated as

previously described (*24*). For the PDGFRαV1/βV2 heterodimer cell line, PDGFRα-V1/pLVX-

Puro (*24*) and PDGFRβ-V2/pLVX-Puro (*24*) lentiviral constructs (10 mg each) and packaging

vectors pCMV-VSV-G (*53*) and pCMV-dR8.91 (*54*) (5 mg each) were transfected into HEK

293T/17 cells (American Type Culture Collection) using Lipofectamine LTX (Thermo Fisher

Scientific, Waltham, MA, USA). For the myristoylated-Venus-HCC15 cell line, the pCAG:myr-

Venus sequence (#32602, Addgene, Watertown, MA, USA) was amplified by PCR using the

following primers (Integrated DNA Technologies, Inc., Coralville, IA, USA): 5'-

GATAGGATCCGCCACCATG-3' and 5'-CGTTTCTAGATTACTTGTACAGCTCG-3'. The

sequence was cloned into the pLVX-Puro vector using BamHI and XbaI sites. The myr-

Venus/pLVX-Puro lentiviral construct (10 mg) and packaging vectors pCMV-VSV-G and

pCMV-dR8.91 (5 mg each) were transfected into HEK 293T/17 cells using Lipofectamine LTX.

In each case, medium containing lentivirus was collected 48 h and 72 h following transfection

and filtered using a 13 mm syringe filter with a 0.45 µm PVDF membrane (Thermo Fisher

Scientific) following addition of 4 mg/ml polybrene (Sigma-Aldrich, St Louis, MO, USA).

Lentiviral-containing medium was added to HCC15 lung cancer cells (see below) every 24 h for

2 days, and cells were subsequently grown in the presence of 2 µg/ml puromycin for 10 days.

Individual Venus-positive cells were isolated on a Moflo XDP 100 cell sorter (Beckman Coulter

Inc., Brea, CA, USA), following 5 min of stimulation with 10 ng/ml PDGF-BB (R&D Systems,

Minneapolis, MN, USA) in the case of the PDGFRαV1/βV2 heterodimer cell line, and expanded

492   to generate clonal cell lines. The final clone chosen for each cell line was confirmed by PCR

493   amplification of the inserted sequence(s) from genomic DNA using primers found in Table S1.

494   These PCR products were subcloned into the Zero Blunt TOPO vector (Thermo Fisher

495   Scientific) and Sanger sequenced.

496

497   **PDGFR-BiFC-HCC15 and myr-Venus-HCC15 cell culture**

498   The HCC15 lung cancer cell line was obtained from the laboratory of Dr. Lynn Heasley

499   (University of Colorado Anschutz Medical Campus). The cell line was authenticated through

500   short tandem repeat analysis and tested for mycoplasma contamination every 10 passages using

501   the MycoAlert Mycoplasma Detection Kit (Lonza Group Ltd, Basel, Switzerland). PDGFR-

502   BiFC and myr-Venus stable cells were cultured in RPMI growth medium [RPMI 1640 (Gibco,

503   Thermo Fisher Scientific) supplemented with 100 U/ml penicillin (Gibco), 100 µg/ml

504   streptomycin (Gibco) containing 10% FBS (Hyclone Laboratories Inc., Logan, UT, USA)] at

505    $37°C$ in 5% CO_2. Once the stable cell lines were established, they were split at a ratio of 1:5 for

506   maintenance. PDGFRα/β heterodimer cells were used for experiments at passages 10-17,

507   PDGFRα homodimer cells were used for experiments at passages 39-44, PDGFRβ homodimer

508   cells were used for experiments at passages 48-53, and myr-Venus cells were used for

509   experiments at passages 10-13. When serum starved, cells were grown in HITES medium

510   [DMEM/F12 (Corning, Corning, NY, USA) supplemented with 0.1% bovine serum albumin

511   (Fisher Scientific, Thermo Fisher Scientific), 10 mM β-estradiol (Sigma-Aldrich), 10 mM

512   hydrocortisone (Sigma-Aldrich), 5 µg/ml insulin (Sigma-Aldrich), 100 U/ml penicillin (Gibco),

513   100 µg/ml streptomycin (Gibco), 1.2 mg/ml $NaHCO_3$ (Santa Cruz Biotechnology, Inc., Dallas,

514   TX, USA), 30 nM Na_3SeO_3 (Sigma-Aldrich) and 10 µg/ml apo-transferrin (Sigma-Aldrich)].

515

qRT-PCR

517   Total RNA was isolated using the RNeasy Mini Kit (Qiagen, Germantown, MD, USA) according

518   to the manufacturer's instructions. First-strand cDNA was synthesized using a ratio of 2:1

519   random primers:oligo (dT) primer and SuperScript II RT (Invitrogen, Thermo Fisher Scientific)

520   according to the manufacturer's instructions. qRT-PCR was performed on a CFX Connect Real-

521   Time PCR Detection System and analyzed with CFX Manager software (version 3.1; Bio-Rad

522   Laboratories, Inc., Hercules, CA, USA). All reactions were performed with SYBR Select Master

523   Mix (Applied Biosystems, Thermo Fisher Scientific), 300 nM primers (Integrated DNA

524   Technologies, Inc.) and cDNA in a 20 µl reaction volume. PCR primers for qRT-PCR analyses

525   can be found in Table S1. The following PCR protocol was used: step 1, 2 min at 50°C; step 2, 2

526   min at 95°C; step 3, 15 s at 95°C; step 4, 1 min at 60°C; repeat steps 3 and 4 for 39 cycles; step 5

527   (melting curve), 5 s per 0.5°C increment from 65°C to 95°C. All samples were run in triplicate

528   and normalized against an endogenous internal control, *B2M*. qRT-PCR experiments were

529   performed across three independent experiments, each using a separate passage of cells.

530

Immunoprecipitations and western blotting

532   PDGFR-BiFC-HCC15 cells and myr-Venus-HCC15 cells were cultured as described above. To

533   induce PDGFRα homodimer, PDGFRα/β heterodimer or PDGFRβ homodimer signaling,

534   PDGFRα homodimer cells and PDGFRβ homodimer cells at ∼60–70% confluence or

535   PDGFRα/β heterodimer cells at ∼70-80% confluence were serum starved for 24 h in HITES

536   medium and stimulated with 10 ng/ml PDGF-AA (PDGFRα homodimer cells) or PDGF-BB

537   (PDGFRα/β heterodimer and PDGFRβ homodimer cells) ligand (R&D Systems) for the

538   indicated length of time. When applicable, cells were transfected with siRNA (see below) for 48

539   h before ligand stimulation. Protein lysates for immunoprecipitation were generated by

540   resuspending cells in ice-cold GFP-Trap buffer [M-PER mammalian protein extraction reagent

541   (Thermo Fisher Scientific), 1x complete Mini protease inhibitor cocktail (Roche,

542   MilliporeSigma, Burlington, MA, USA), 1 mM PMSF, 10mM NaF, 1 mM Na_3VO_4, 25 mM β-

543   glycerophosphate] and collecting cleared lysates by centrifugation at 13,400 g at 4°C for 20 min.

544   For immunoprecipitations, cell lysates (500 µg for PDGFRα homodimers and PDGFRβ

545   homodimers, 1 mg for PDGFRα/β heterodimers) were incubated with GFP-Trap agarose beads

546   (Bulldog Bio, Inc., Portsmouth, NH, USA) for 1 h at 4°C. Beads were washed three times with

547   ice-cold GFP-Trap buffer and the precipitated proteins were eluted with Laemmli buffer

548   containing 10% β-mercaptoethanol, heated for 10 min at 100°C and separated by SDS-PAGE.

549   When applicable, supernatant from immunoprecipitation experiments was incubated with

550   primary antibody overnight at 4°C followed by incubation with 20 µL of Protein A/G Plus-

551   agarose beads (Santa Cruz Biotechnology, Inc.) for 2 h at 4°C the following day. Beads were

552   washed five times with ice-cold GFP-Trap buffer and the precipitated proteins were eluted with

553   Laemmli buffer containing 10% β-mercaptoethanol, heated for 5 min at 95°C, and separated by

554   SDS-PAGE. For western blotting analysis of whole-cell lysates, protein lysates were generated

555   by resuspending cells in ice-cold GFP-Trap buffer and collecting cleared lysates by

556   centrifugation at 13,400 g at 4°C for 20 min. Laemmli buffer containing 10% β-mercaptoethanol

557   was added to the lysates, which were heated for 5 min at 100°C. Proteins were subsequently

558   separated by SDS-PAGE. Western blot analysis was performed according to standard protocols

559   using horseradish peroxidase-conjugated secondary antibodies. Blots were imaged using a

560   ChemiDoc XRS+ (Bio-Rad Laboratories, Inc.) or a ChemiDoc (Bio-Rad Laboratories, Inc.). The

561   following antibodies were used for western blotting: PDGFRα (1:1000; D13C6; 5241; Cell

562   Signaling Technology, Inc., Danvers, MA, USA); PDGFRβ (1:1000; 28E1; 3169; Cell Signaling

563   Technology, Inc.); β-tubulin (1:1000; E7; E7; Developmental Studies Hybridoma Bank, Iowa

564   City, IA, USA); Lamin B1 (1:1000; D4Q4Z, 12586; Cell Signaling Technology Inc.); phospho-

565   PDGFRα (Tyr 849)/PDGFRβ (Tyr857) (1:1000; C43E9; 3170; Cell Signaling Technology, Inc.);

566   phospho-ERK1/2 (Thr202/Tyr204) (1:1000; 9101; Cell Signaling Technology, Inc.); ERK1/2

567   (1:1000; 9102; Cell Signaling Technology, Inc.); phospho-AKT (Ser473) (1:1000; 9271; Cell

568   Signaling Technology Inc.); AKT (1:1000; 9272; Cell Signaling Technology Inc.); Myosin ID

569   (1:500; H-1; sc-515292; Santa Cruz Biotechnology, Inc); GAPDH (1:50000; 1E6D9; 60004-1-

570   Ig; Proteintech Group Inc, Rosemont, IL, USA); horseradish peroxidase-conjugated goat anti-

571   rabbit IgG (1:20,000; 111035003; Jackson ImmunoResearch Inc., West Grove, PA, USA); and

572   horseradish peroxidase-conjugated goat anti-mouse IgG (1:20,000; 115035003; Jackson

573   ImmunoResearch Inc.). Quantifications of signal intensity were performed with ImageJ software

574   (version 1.53t, National Institutes of Health, Bethesda, MD, USA). Relative dimerized PDGFR

575   levels were determined by normalizing GFP-Trap immunoprecipitated PDGFR levels to total

576   PDGFR levels. Relative phospho-PDGFR levels were determined by normalizing to total

577   PDGFR levels, except for ligand sink experiments in which relative phospho-PDGFR levels

578   were determined by normalizing to unstimulated phospho-PDGFR signals. Relative phospho-

579   ERK1/2 levels were determined by normalizing to total ERK1/2 levels. Relative phospho-AKT

580   levels were determined by normalizing to total AKT levels. When applicable, statistical analyses

581   were performed with Prism 9 (GraphPad Software Inc., San Diego, CA, USA) using a two-

582   tailed, ratio paired *t*-test within each cell line (comparing individual ligand treatment timepoint

583   values to the no ligand 0 min timepoint value) or a two-tailed, unpaired *t*-test with Welch's

584   correction between each treatment. Immunoprecipitation and western blotting experiments were

585   performed across three independent experiments.

586

587   **Fluorescence analysis**

588   For fluorescence intensity and marker colocalization experiments, cells were seeded onto glass

589   coverslips coated with 5 µg/ml human plasma fibronectin purified protein (MilliporeSigma) at a

590   density of 80,000 cells, 100,000 cells and 40,000 cells per 24-well plate well for the PDGFRα

591   homodimer cell line, the PDGFRα/β heterodimer cell line and the PDGFRβ homodimer cell line,

592   respectively, in RPMI growth medium. After 24 h, cells were washed with 1x phosphate

593   buffered saline (PBS) and serum starved in HITES medium. HITES medium was replaced 23 h

594   later. After 54 min, coverslips were photobleached for 1 min with an Axio Observer 7

595   fluorescence microscope (Carl Zeiss Microscopy LLC, White Plains, NY, USA) using the 2.5x

596   objective and 488 nm laser. Cells were allowed to recover for 5 min and were treated with 10

597   ng/ml PDGF-AA (PDGFRα homodimer cells) or PDGF-BB (PDGFRα/β heterodimer and

598   PDGFRβ homodimer cells) ligand (R&D Systems) for the indicated amount of time. When

599   applicable, cells were transfected with siRNA (see below) for 48 h before ligand stimulation.

600   Cells were fixed in 4% paraformaldehyde (PFA) in PBS with 0.1% Triton X-100 for 10 min and

601   washed in PBS. Cells were blocked for 1 h in 5% normal donkey serum (Jackson

602   ImmunoResearch Inc.) in PBS and incubated overnight at 4°C in primary antibody diluted in 1%

603   normal donkey serum in PBS. After washing in PBS, cells were incubated in Alexa Fluor 546-

604   conjugated donkey anti-rabbit secondary antibody (1:1000; A21206; Invitrogen) or Alexa Fluor

605   546-conjugated donkey anti-mouse secondary antibody (1:1000; A10036; Invitrogen) diluted in

606   1% normal donkey serum in PBS with 2 µg/ml DAPI (Sigma-Aldrich) for 1 h. Cells were

27

607   mounted in VECTASHIELD HardSet Antifade Mounting Medium (Vector Laboratories, Inc.,

608   Burlingame, CA, USA) and photographed using an Axiocam 506 mono digital camera (Carl

609   Zeiss Microscopy LLC) fitted onto an Axio Observer 7 fluorescence microscope (Carl Zeiss

610   Microscopy LLC) with the 63x oil objective with a numerical aperture of 1.4 at room

611   temperature. The following antibodies were used for immunofluorescence analysis: PDGFRα

612   (1:1000; D13C6; 5241; Cell Signaling Technology, Inc.); PDGFRβ (1:1000; 28E1; 3169; Cell

613   Signaling Technology, Inc.); Na$^+$/K$^+$-ATPase (1:500; EP1845Y; ab76020; Abcam); RAB5

614   (1:200; C8B1; 3547; Cell Signaling Technology Inc.); APPL1 (1:200; D83H4; 3858; Cell

615   Signaling Technology Inc.); EEA1 (1:200; C45B10; 3288; Cell Signaling Technology Inc.);

616   RAB7 (1:100; D95F2; 9367; Cell Signaling Technology Inc.); RAB4 (1:200; ab13252; Abcam);

617   RAB11 (1:100; D4F5; 5589; Cell Signaling Technology Inc.) and Myosin ID (1:500; H-1; sc-

618   515292; Santa Cruz Biotechnology, Inc). For fluorescence intensity measurements, three

619   independent trials, or biological replicates, were performed. For each biological replicate, at least

620   38 technical replicates consisting of individual cells were imaged with Z-stacks (0.24 μm

621   between Z-stacks with a range of 2-8 Z-stacks). For marker colocalization experiments, three

622   independent trials, or biological replicates, were performed. For each biological replicate, at least

623   10 technical replicates consisting of individual cells were imaged with Z-stacks (0.24 μm

624   between Z-stacks with a range of 2-8 Z-stacks) per timepoint. Images were deconvoluted using

625   ZEN Blue software (Carl Zeiss Microscopy LLC) using the 'Better, fast (Regularized Inverse

626   Filter)' setting. For all images, extended depth of focus was applied to Z-stacks using ZEN Blue

627   software (Carl Zeiss Microscopy LLC) to generate images with the maximum depth of field. For

628   fluorescence intensity measurements, background was subtracted using rolling background

629   subtraction with a radius of 30 pixels using Fiji software (version 2.1.0/1.53c). A region of

28

630 interest (ROI) was drawn around each Venus-positive cell, and integrated density was measured

631 and recorded as the fluorescence intensity. For marker colocalization measurements, an ROI was

632 drawn around each Venus-positive cell in the corresponding Cy3 (marker) channel using Fiji

633 software (version 2.1.0/1.53c). For each image with a given ROI, the Cy3 channel and the EGFP

634 channel were converted to 8-bit images. Colocalization was measured using the Colocalization

635 Threshold function, where the rcoloc value [Pearson's correlation coefficient (PCC)] was used in

636 statistical analysis. When applicable, statistical analyses were performed on the average values

637 from each biological replicate with Prism 9 (GraphPad Software Inc.) using a two-tailed,

638 paired t-test within each cell line (comparing individual ligand treatment timepoint values to the

639 no ligand 0 min timepoint value) or a two-tailed, unpaired t-test with Welch's correction between

640 each cell line, siRNA treatment or non-0 min ligand treatment timepoints.

641

642 **Anchorage-independent growth assays**

643 For measurement of anchorage-independent cell growth, 25,000 cells were suspended in 1.5 ml

644 RPMI growth medium with 0.35% Difco Agar Noble (Becton, Dickinson and Company,

645 Franklin Lakes, NJ) and overlaid on a base layer containing 1.5 ml RPMI growth medium with

646 0.5% Difco Agar Noble (Becton, Dickinson and Company) in six-well plate wells. A feeding

647 layer of 2 ml RPMI growth medium supplemented with 10 ng/ml PDGF-BB ligand (R&D

648 Systems) and/or 0.01 uM siRNA (see below) was added on top of the agar and replaced every

649 day. Plates were incubated at 37°C in 5% CO_2 for 10 days, and viable colonies were stained

650 overnight with 1 mg/ml Nitrotetrazoleum Blue (Sigma-Aldrich) in PBS at 37°C. Following a

651 second overnight incubation at 4°C, wells from each independent trial were photographed using

652 a COOLPIX S600 digital camera (Nikon Inc., Melville, NY, USA). Images were made binary

29

653 using Adobe Photoshop (version 25.0.1; Adobe Inc., San Jose, CA, USA), and colony number

654 and area were quantified using MetaMorph imaging software (Molecular Devices, LLC, San

655 Jose, CA, USA). Statistical analyses were performed on values from each of three independent

656 trials, or biological replicates, with Prism 9 (GraphPad Software Inc.) using a two-tailed,

657 paired *t*-test within each cell line or siRNA treatment and a two-tailed, unpaired *t*-test with

658 Welch's correction between each cell line or siRNA treatment.

659

Mass spectrometry

661 The following amino acids were used for stable isotope labeling: unlabeled (light) L-

662 LYSINE:2HCL, unlabeled (light) L-ARGININE:HCL, stable isotope-labeled (heavy) L-

663 LYSINE:2HCL (13C6, 99%;15N2, 99%) and stable isotope-labeled (heavy) L-ARGININE:HCL

664 (13C6, 99%; 15N4, 99%) (Cambridge Isotope Labs, Inc. Andover, MA). Light SILAC medium

665 was generated by adding unlabeled L-LYSINE:2HCL (final concentration 146.0 mg/mL) and

666 unlabeled L-ARGININE:HCL (final concentration 42.0 mg/mL) to RPMI SILAC growth

667 medium [RPMI 1640 SILAC (Gibco, Thermo Fisher Scientific) supplemented with 100 U/ml

668 penicillin (Gibco), 100 µg/ml streptomycin (Gibco) containing 10% FBS (Hyclone Laboratories

669 Inc.)]. Heavy isotope SILAC medium was generated by adding heavy labeled L-LYSINE:2HCL

670 (13C6, 99%;15N2, 99%) (final concentration 151.3 mg/mL) and heavy labeled L-

671 ARGININE:HCL (13C6, 99%; 15N4, 99%) (final concentration 44.0 mg/mL) in RPMI SILAC

672 growth medium. Each SILAC medium was filtered through a 0.22-um syringe filter. Each

673 PDGFR-BiFC cell line was cultured in duplicate in light SILAC medium and separately in heavy

674 SILAC medium for at least 6 cell passages to achieve >95% labeling. PDGFRα homodimer cells

675 at ~75% confluence, PDGFRα/β heterodimer cells at ~70-80% confluence and PDGFRβ

676   homodimer cells at ~65% confluence were serum starved for 24 h in HITES medium. Cells

677   grown in light SILAC medium were left unstimulated and cells grown in heavy SIILAC medium

678   were stimulated with 10 ng/ml PDGF-AA (PDGFRα homodimer cells) or 10 ng/ml of PDGF-BB

679   (PDGFRα/β heterodimer and PDGFRβ homodimer cells) ligand for 5 minutes. Myr-Venus cells

680   were cultured in light SILAC medium, serum starved at ~70% confluence for 24 h in HITES

681   medium and left unstimulated. Protein lysates for immunoprecipitation were generated by

682   resuspending cells in ice-cold GFP-Trap buffer and collecting cleared lysates by centrifugation at

683   13,400 g at 4°C for 20 min. Before immunoprecipitation, light SILAC samples were combined

684   with heavy SILAC samples in a 1:1 ratio per cell line. For immunoprecipitations, cell lysates

685   (500 μg for myr-Venus, PDGFRα homodimers and PDGFRβ homodimers, 1 mg for PDGFRα/β

686   heterodimers) were incubated with GFP-Trap agarose beads (Bulldog Bio, Inc.) for 1 h at 4°C.

687   Beads were washed three times with ice-cold GFP-Trap buffer.

688   To prepare for trypsin digestion, beads were resuspended with 8 M urea, 50 mM

689   ammonium bicarbonate. Tris (2-carboxyethyl)phosphine (TCEP) was added to a final

690   concentration of 10 mM and samples were incubated at 30°C for 1 h. Alkylation was performed

691   by adding chloroacetamide (CAA) to 25 mM and incubating in the dark at room temperature for

692   30 min. Following alkylation, urea was diluted to 1 M and proteins digested overnight with

693   modified sequencing grade trypsin (Promega, Madison, WI, USA) at a 1:50 enzyme:protein

694   ratio. Beads were then centrifuged for 15 min at 18,000 g and supernatant digest solution was

695   collected. Digested peptides were then desalted using Pierce C18 spin tips (Thermo Fisher

696   Scientific) according to the manufacturer's instructions.

697   Digested peptides were loaded onto individual Evotips (Evosep Biosystems, Odense,

698   Denmark) following the manufacturer's instructions and separated on an Evosep One

699   chromatography system (Evosep Biosystems) using a Pepsep column (150 μm inter diameter, 15

700   cm) packed with ReproSil C18 1.9 μm, 120Å resin. Samples were analyzed using the instrument

701   default "30 samples per day" LC gradient. The system was coupled to the timsTOF Pro mass

702   spectrometer (Bruker Daltonics, Bremen, Germany) via the nano-electrospray ion source

703   (Captive Spray, Bruker Daltonics). The mass spectrometer was operated in PASEF mode. The

704   ramp time was set to 100 ms and 10 PASEF MS/MS scans per topN acquisition cycle were

705   acquired. MS and MS/MS spectra were recorded from m/z 100 to 1700. The ion mobility was

706   scanned from 0.7 to 1.50 Vs/cm2. Precursors for data-dependent acquisition were isolated

707   within ± 1 Th and fragmented with an ion mobility-dependent collision energy, which was

708   linearly increased from 20 to 59 eV in positive mode. Low-abundance precursor ions with an

709   intensity above a threshold of 500 counts but below a target value of 20000 counts were

710   repeatedly scheduled and otherwise dynamically excluded for 0.4 min.

711   Data was searched using PEAKS X Pro version 10.6 (Bioinformatics Solutions, Inc.,

712   Ontario, Canada). Precursor tolerance was set to ±25 ppm and fragment tolerance was set to ±0.2

713   Da. Data was searched against SwissProt (20,379 sequences) restricted to *Homo sapiens*. Each

714   fraction was searched independently using a fully specific trypsin cleavage definition allowing

715   for 2 missed cleavages and a maximum of 5 modifications per peptide. Fixed modifications were

716   set as carbamidomethyl (C). Variable modifications were set as oxidation (M), acetylation (K,

717   protein N-term), and phosphorylation (STY). SILAC isotope modifications 13C(6) 15N(4) (R)

718   and 13C(6) 15N(2) (K) were also set as variable modifications. Results were filtered to 1% FDR

719   at the peptide and protein level. SILAC quantification was performed using a "Quantification"

720   task in PEAKS X Pro set for SILAC 2-plex (R10, K8) analysis. Quantification retention time

721   range was set to 1.0 minute, with an ion mobility range of 0.05 1/k0. Heavy conditions were set

722   to include 100% R(+10.01) and K(+8.01) modifications. All results were filtered to 1% FDR.

723   Auto-normalization was applied to the quantification results within PEAKS before further

724   processing.

725

726   **siRNA-mediated knockdown of Myosin ID**

727   PDGFRα/β heterodimer cells at ~60% confluence were transfected with Silencer Select Negative

728   Control No. 1 siRNA (4390843; Invitrogen, Thermo Fisher Scientific) and separately two

729   Silencer Select siRNAs targeting human Myosin ID (4392420; ID s9203 and s9204; Invitrogen,

730   Thermo Fisher Scientific) at a final concentration of 0.01 uM using Lipofectamine RNAiMAX

731   (Invitrogen, Thermo Fisher Scientific) according to the manufacturer's instructions for the

732   indicated amount of time.

733

734   **Supplementary Materials**

735   **Fig. S1. Validation of a PDGFRα/β-BiFC stable cell line.**

736   **Fig. S2. PDGFRα/β heterodimers are ultimately trafficked for degradation and recycling.**

737   **Fig. S3. PDGFRα/β heterodimers may serve as ligand sinks.**

738   **Fig. S4. Gene ontology analysis of proteins that interact with the various PDGFR dimers.**

739   **Fig. S5. *MYO1D* expression is upregulated in the PDGFRα/β heterodimer cell line.**

740   **Fig. S6. Knockdown of MYO1D in the PDGFRα/β heterodimer cell line.**

741   **Table S1. PCR primers for confirmation of sequence integration and qRT-PCR analyses.**

742

743   **References and Notes**

744   1.   C. H. Heldin, B. Westermark, Mechanism of action and in vivo role of platelet-derived

745   growth factor. *Physiol Rev* **79**, 1283-1316 (1999).

746   2.   R. V. Hoch, P. Soriano, Roles of PDGF in animal development. *Development* **130**, 4769-

747   4784 (2003).

748   3.   L. T. Williams, Signal transduction by the platelet-derived growth factor receptor. *Science*

749   **243**, 1564-1570 (1989).

750   4.   T. Matsui *et al.*, Isolation of a novel receptor cDNA establishes the existence of two

751   PDGF receptor genes. *Science* **243**, 800-804 (1989).

752   5.   R. A. Seifert *et al.*, Two different subunits associate to create isoform-specific platelet-

753   derived growth factor receptors. *J Biol Chem* **264**, 8771-8778 (1989).

754   6.   B. Herren *et al.*, Dimerization of extracellular domains of platelet-derived growth factor

755   receptors. A revised model of receptor-ligand interaction. *J Biol Chem* **268**, 15088-15095

756   (1993).

757   7.   A. H. Shim *et al.*, Structures of a platelet-derived growth factor/propeptide complex and a

758   platelet-derived growth factor/receptor complex. *Proc Natl Acad Sci U S A* **107**, 11307-

759   11312 (2010).

760   8.   K. A. Fantauzzo, P. Soriano, PDGFRbeta regulates craniofacial development through

761   homodimers and functional heterodimers with PDGFRalpha. *Genes Dev* **30**, 2443-2458

762   (2016).

763   9.   J. D. Kelly *et al.*, Platelet-derived growth factor (PDGF) stimulates PDGF receptor

764   subunit dimerization and intersubunit trans-phosphorylation. *J Biol Chem* **266**, 8987-

765   8992 (1991).

766 10. H. Bostrom *et al.*, PDGF-A signaling is a critical event in lung alveolar myofibroblast

767   development and alveogenesis. *Cell* **85**, 863-873 (1996).

768 11. P. Soriano, The PDGF alpha receptor is required for neural crest cell development and for

769   normal patterning of the somites. *Development* **124**, 2691-2700 (1997).

770 12. H. Ding *et al.*, A specific requirement for PDGF-C in palate formation and PDGFR-alpha

771   signaling. *Nat Genet* **36**, 1111-1116 (2004).

772 13. P. Leveen *et al.*, Mice deficient for PDGF B show renal, cardiovascular, and

773   hematological abnormalities. *Genes Dev* **8**, 1875-1887 (1994).

774 14. P. Soriano, Abnormal kidney development and hematological disorders in PDGF beta-

775   receptor mutant mice. *Genes Dev* **8**, 1888-1896 (1994).

776 15. H. Gladh *et al.*, Mice Lacking Platelet-Derived Growth Factor D Display a Mild Vascular

777   Phenotype. *PLoS One* **11**, e0152276 (2016).

778 16. R. A. Klinghoffer, T. G. Hamilton, R. Hoch, P. Soriano, An allelic series at the

779   PDGFalphaR locus indicates unequal contributions of distinct signaling pathways during

780   development. *Dev Cell* **2**, 103-113 (2002).

781 17. J. C. Yu *et al.*, Tyrosine mutations within the alpha platelet-derived growth factor receptor

782   kinase insert domain abrogate receptor-associated phosphatidylinositol-3 kinase activity

783   without affecting mitogenic or chemotactic signal transduction. *Mol Cell Biol* **11**, 3780-

784   3785 (1991).

785 18. R. Heuchel *et al.*, Platelet-derived growth factor beta receptor regulates interstitial fluid

786   homeostasis through phosphatidylinositol-3' kinase signaling. *Proc Natl Acad Sci U S A*

787   **96**, 11410-11415 (1999).

35

788   19.   N. McCarthy *et al.*, Pdgfra and Pdgfrb genetically interact during craniofacial

789   development. *Dev Dyn* **245**, 641-652 (2016).

790   20.   K. A. Fantauzzo, P. Soriano, Generation of an immortalized mouse embryonic palatal

791   mesenchyme cell line. *PLoS One* **12**, e0179078 (2017).

792   21.   J. Mo, R. Long, K. A. Fantauzzo, Pdgfra and Pdgfrb Genetically Interact in the Murine

793   Neural Crest Cell Lineage to Regulate Migration and Proliferation. *Front Physiol* **11**,

794   588901 (2020).

795   22.   C. D. Hu, Y. Chinenov, T. K. Kerppola, Visualization of interactions among bZIP and Rel

796   family proteins in living cells using bimolecular fluorescence complementation. *Mol Cell*

797   **9**, 789-798 (2002).

798   23.   Y. J. Shyu, H. Liu, X. Deng, C. D. Hu, Identification of new fluorescent protein

799   fragments for bimolecular fluorescence complementation analysis under physiological

800   conditions. *Biotechniques* **40**, 61-66 (2006).

801   24.   M. A. Rogers, M. B. Campana, R. Long, K. A. Fantauzzo, PDGFR dimer-specific

802   activation, trafficking and downstream signaling dynamics. *J Cell Sci* **135**, (2022).

803   25.   D. R. Croucher *et al.*, Bimolecular complementation affinity purification (BiCAP) reveals

804   dimer-specific protein interactions for ERBB2 dimers. *Sci Signal* **9**, ra69 (2016).

805   26.   J. Barretina *et al.*, The Cancer Cell Line Encyclopedia enables predictive modelling of

806   anticancer drug sensitivity. *Nature* **483**, 603-607 (2012).

807   27.   C. Cancer Cell Line Encyclopedia, C. Genomics of Drug Sensitivity in Cancer,

808   Pharmacogenomic agreement between two cancer cell line data sets. *Nature* **528**, 84-87

809   (2015).

810 28. Y. Yang, P. Xie, Y. Opatowsky, J. Schlessinger, Direct contacts between extracellular
811   membrane-proximal domains are required for VEGF receptor activation and cell
812   signaling. *Proc Natl Acad Sci U S A* **107**, 1906-1911 (2010).

813 29. S. Mori, K. Tanaka, S. Omura, Y. Saito, Degradation process of ligand-stimulated
814   platelet-derived growth factor beta-receptor involves ubiquitin-proteasome proteolytic
815   pathway. *J Biol Chem* **270**, 29447-29452 (1995).

816 30. S. Miyake, M. L. Lupher, Jr., B. Druker, H. Band, The tyrosine kinase regulator Cbl
817   enhances the ubiquitination and degradation of the platelet-derived growth factor receptor
818   alpha. *Proc Natl Acad Sci U S A* **95**, 7927-7932 (1998).

819 31. S. Miyake, K. P. Mullane-Robinson, N. L. Lill, P. Douillard, H. Band, Cbl-mediated
820   negative regulation of platelet-derived growth factor receptor-dependent cell
821   proliferation. A critical role for Cbl tyrosine kinase-binding domain. *J Biol Chem* **274**,
822   16619-16628 (1999).

823 32. S. Karlsson *et al.*, Loss of T-cell protein tyrosine phosphatase induces recycling of the
824   platelet-derived growth factor (PDGF) beta-receptor but not the PDGF alpha-receptor.
825   *Mol Biol Cell* **17**, 4846-4855 (2006).

826 33. C. Hellberg, C. Schmees, S. Karlsson, A. Ahgren, C. H. Heldin, Activation of protein
827   kinase C alpha is necessary for sorting the PDGF beta-receptor to Rab4a-dependent
828   recycling. *Mol Biol Cell* **20**, 2856-2863 (2009).

829 34. J. C. Skou, The identification of the sodium-pump as the membrane-bound Na+/K+-
830   ATPase: a commentary on 'The Influence of Some Cations on an Adenosine
831   Triphosphatase from Peripheral Nerves'. *Biochim Biophys Acta* **1000**, 435-438 (1989).

832   35.   M. Zerial, H. McBride, Rab proteins as membrane organisers. *Nature Reviews Molecular*
833   *Cell Biology* **2**, 107-117 (2001).

834   36.   M. Miaczynska *et al.*, APPL proteins link Rab5 to nuclear signal transduction via an
835   endosomal compartment. *Cell* **116**, 445-456 (2004).

836   37.   F. T. Mu *et al.*, EEA1, an early endosome-associated protein. EEA1 is a conserved alpha-
837   helical peripheral membrane protein flanked by cysteine "fingers" and contains a
838   calmodulin-binding IQ motif. *J Biol Chem* **270**, 13503-13511 (1995).

839   38.   H. N. Vasudevan, P. Mazot, F. He, P. Soriano, Receptor tyrosine kinases modulate distinct
840   transcriptional programs by differential usage of intracellular pathways. *Elife* **4**, e07186
841   (2015).

842   39.   F. He, P. Soriano, A critical role for PDGFRalpha signaling in medial nasal process
843   development. *PLoS Genet* **9**, e1003851 (2013).

844   40.   F. He, P. Soriano, Sox10ER(T2) CreER(T2) mice enable tracing of distinct neural crest
845   cell populations. *Dev Dyn* **244**, 1394-1403 (2015).

846   41.   D. Mellacheruvu *et al.*, The CRAPome: a contaminant repository for affinity purification-
847   mass spectrometry data. *Nat Methods* **10**, 730-736 (2013).

848   42.   Z. Xie *et al.*, Gene Set Knowledge Discovery with Enrichr. *Curr Protoc* **1**, e90 (2021).

849   43.   Y. S. Ko *et al.*, MYO1D binds with kinase domain of the EGFR family to anchor them to
850   plasma membrane before their activation and contributes carcinogenesis. *Oncogene* **38**,
851   7416-7432 (2019).

852   44.   S. P. Kennedy *et al.*, Targeting promiscuous heterodimerization overcomes innate
853   resistance to ERBB2 dimerization inhibitors in breast cancer. *Breast Cancer Res* **21**, 43
854   (2019).

855 45. D. C. Lin *et al.*, APPL1 associates with TrkA and GIPC1 and is required for nerve growth
856 factor-mediated signal transduction. *Mol Cell Biol* **26**, 8928-8941 (2006).
857 46. T. Varsano *et al.*, GIPC is recruited by APPL to peripheral TrkA endosomes and regulates
858 TrkA trafficking and signaling. *Mol Cell Biol* **26**, 8942-8952 (2006).
859 47. R. Zoncu *et al.*, A phosphoinositide switch controls the maturation and signaling
860 properties of APPL endosomes. *Cell* **136**, 1110-1121 (2009).
861 48. J. R. Lee *et al.*, Adaptor protein containing PH domain, PTB domain and leucine zipper
862 (APPL1) regulates the protein level of EGFR by modulating its trafficking. *Biochem*
863 *Biophys Res Commun* **415**, 206-211 (2011).
864 49. K. A. Fantauzzo, P. Soriano, PI3K-mediated PDGFRalpha signaling regulates survival
865 and proliferation in skeletal development through p53-dependent intracellular pathways.
866 *Genes Dev* **28**, 1005-1017 (2014).
867 50. B. J. C. Dennison, E. D. Larson, R. Fu, J. Mo, K. A. Fantauzzo, Srsf3 mediates
868 alternative RNA splicing downstream of PDGFRalpha signaling in the facial
869 mesenchyme. *Development* **148**, (2021).
870 51. H. N. Vasudevan, P. Soriano, SRF regulates craniofacial development through selective
871 recruitment of MRTF cofactors by PDGF signaling. *Dev Cell* **31**, 332-344 (2014).
872 52. A. De Donatis *et al.*, Proliferation versus migration in platelet-derived growth factor
873 signaling: the key role of endocytosis. *J Biol Chem* **283**, 19948-19956 (2008).
874 53. S. A. Stewart *et al.*, Lentivirus-delivered stable gene silencing by RNAi in primary cells.
875 *RNA* **9**, 493-501 (2003).
876 54. R. Zufferey, D. Nagy, R. J. Mandel, L. Naldini, D. Trono, Multiply attenuated lentiviral
877 vector achieves efficient gene delivery in vivo. *Nat Biotechnol* **15**, 871-875 (1997).
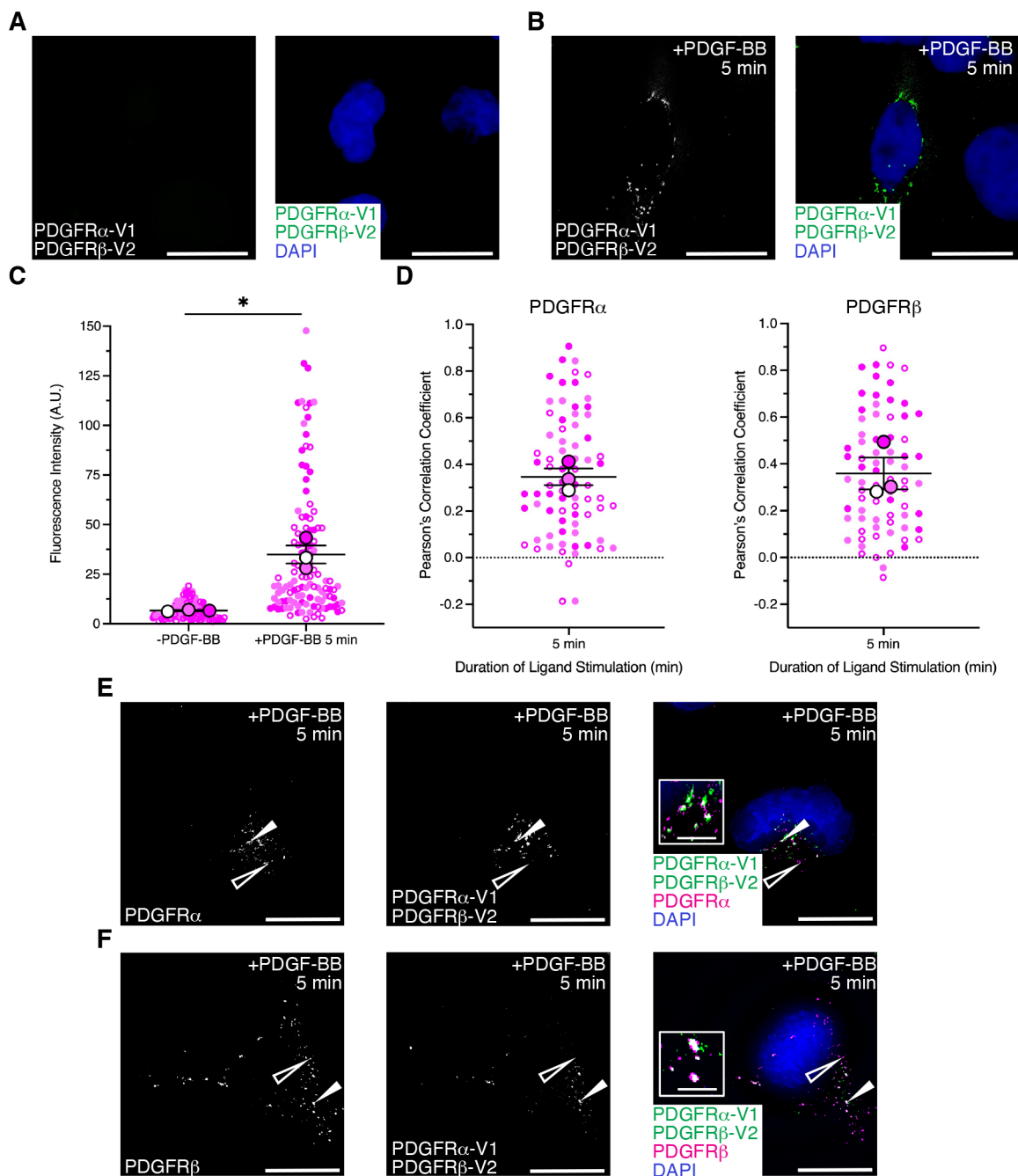
Fig. 1. Validation of a PDGFRα/β-BiFC stable cell line. (**A,B**) Venus expression (white or green) as assessed by fluorescence analysis of HCC15 cells transduced with PDGFRα-V1 and PDGFRβ-V2 in the absence (A) or presence (B) of PDGF-BB ligand for 5 min. Nuclei were stained with DAPI (blue; A,B). Scale bars: 20 μm. (**C**) Scatter dot plot depicting fluorescence intensity for the PDGFRα/β heterodimer cell line in the absence or presence of PDGF-BB ligand

901 for 5 min. Data are mean±s.e.m. *$P<0.05$ (two-tailed, paired *t*-test). Colored circles correspond

902 to independent experiments. Summary statistics from biological replicates consisting of

903 independent experiments (large circles) are superimposed on top of data from all cells; $n \geq 38$

904 technical replicates across each of three biological replicates. (**D**) Scatter dot plots depicting

905 Pearson's correlation coefficient of the PDGFRα/β heterodimer cell line with an anti-PDGFRα

906 antibody (left) and an anti-PDGFRβ antibody (right) following PDGF-BB ligand stimulation for

907 5 min. Data are mean±s.e.m. Colored circles correspond to independent experiments. Summary

908 statistics from biological replicates consisting of independent experiments (large circles) are

909 superimposed on top of data from all cells; $n=25$ technical replicates across each of three

910 biological replicates. (**E,F**) PDGFRα (E) and PDGFRβ (F) antibody signal (white or magenta;

911 E,F) and/or Venus expression (white or green; E,F) as assessed by (immuno)fluorescence

912 analysis of the PDGFRα/β heterodimer cell line. Insets in E and F are regions where white

913 arrows are pointing. Nuclei were stained with DAPI (blue; E,F). White arrows denote

914 colocalization; white outlined arrows denote lack of colocalization. Scale bars: 20 μm (main
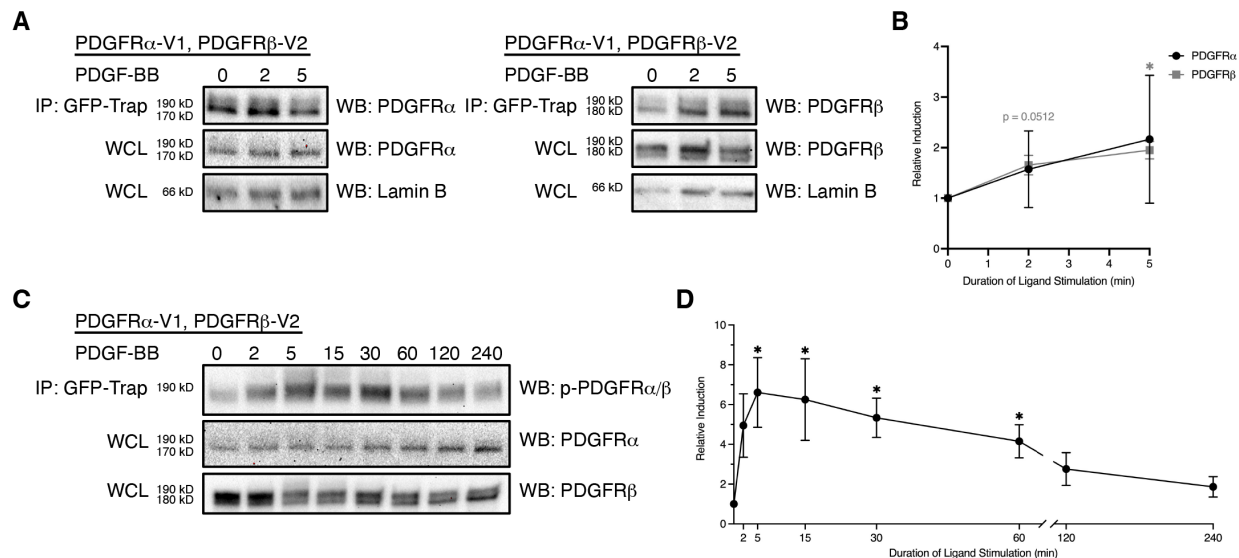
915 images), 3 μm (insets).

916

917

Fig. 2. PDGFRα/β heterodimers dimerize relatively quickly and have peak levels of autophosphorylation following 5 minutes of ligand treatment. (**A**) Immunoprecipitation (IP) of dimerized PDGFRα/β receptors with GFP-Trap nanobody from cells that were unstimulated or treated with PDGF-BB ligand for 2–5 min followed by western blotting (WB) with an anti-PDGFRα (left) or an anti-PDGFRβ antibody (right). WCL, whole-cell lysates. (**B**) Line graph depicting quantification of band intensities from *n*=3 biological replicates as in A. Data are mean±s.e.m. *P<0.05 (two-tailed, ratio paired *t*-test). (**C**) Immunoprecipitation of dimerized PDGFRα/β receptors with GFP-Trap nanobody from cells that were unstimulated or treated with PDGF-BB ligand for 2 min to 4 h followed by western blotting with an anti-phospho (p)-PDGFR antibody. (**D**) Line graph depicting quantification of band intensities from *n*=3 biological replicates as in C. Data are mean±s.e.m. *P<0.05; (two-tailed, ratio paired *t*-test).
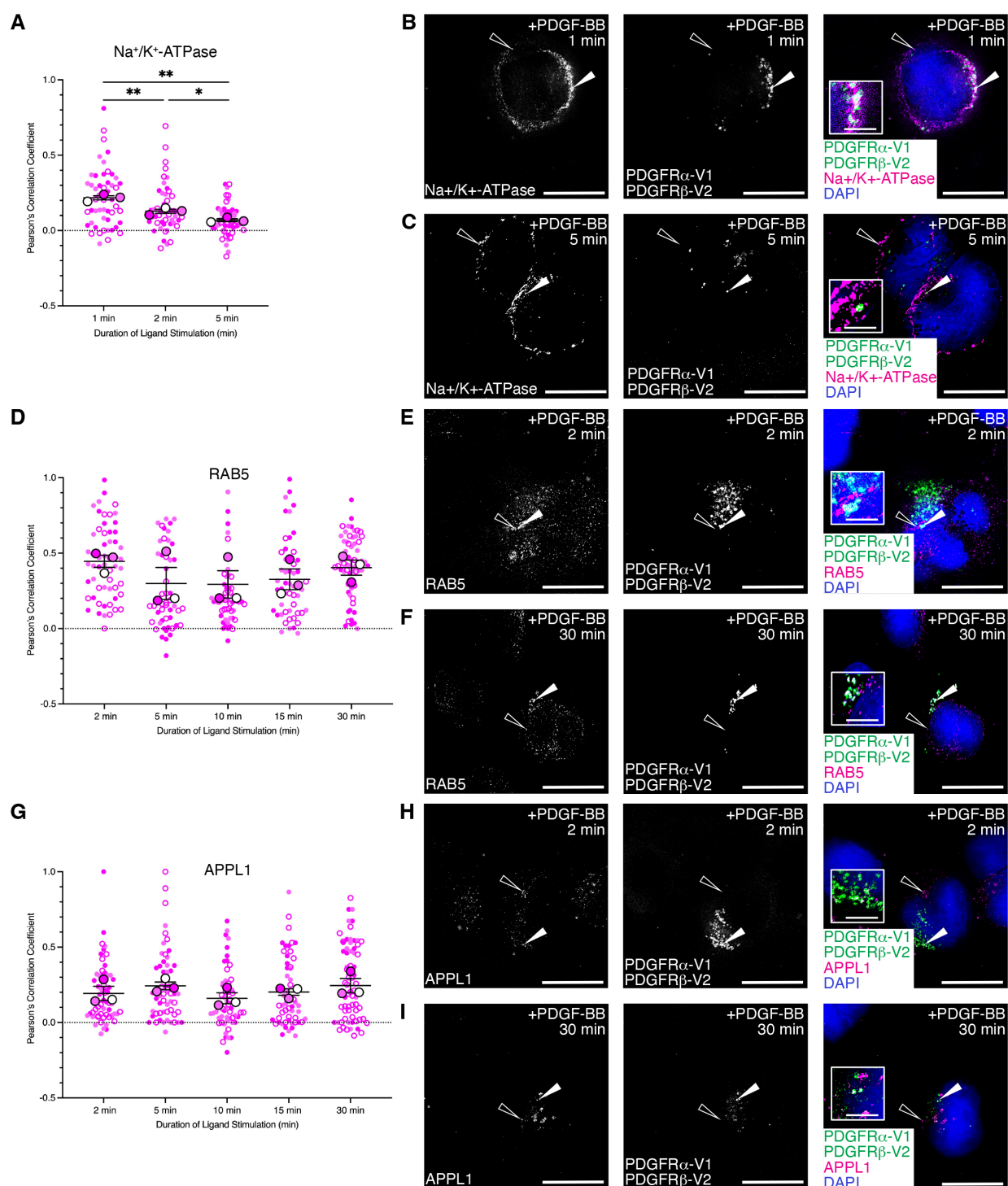
929

43

930

Fig. 3. PDGFRα/β heterodimers are rapidly internalized into signaling endosomes. (A,D,G)

Scatter dot plots depicting Pearson's correlation coefficient of the PDGFRα/β heterodimer cell

line Venus signal with an anti-Na$^+$/K$^+$-ATPase antibody (A), an anti-RAB5 antibody (D) or an

934   anti-APPL1 antibody (G) signal following PDGF-BB ligand stimulation from 1–5 min (A) or 2-

935   30 min (D,G). Data are mean±s.e.m. *$P<0.05$; **$P<0.01$ (two-tailed, unpaired t-test with Welch's

936   correction). Colored circles correspond to independent experiments. Summary statistics from

937   biological replicates consisting of independent experiments (large circles) are superimposed on

938   top of data from all cells; $n \geq 11$ technical replicates across each of three biological replicates.

939   (**B,C,E,F,H,I**) Na^+/K^+-ATPase antibody signal (white or magenta; B,C), RAB5 antibody signal

940   (white or magenta; E,F) or APPL1 antibody signal (white or magenta; H,I) and/or Venus

941   expression (white or green; B,C,E,F,H,I) as assessed by (immuno)fluorescence analysis of the

942   PDGFRα/β heterodimer cell line. Insets in B, C, E, F, H and I are regions where white arrows are

943   pointing. Nuclei were stained with DAPI (blue; B,C,E,F,H,I). White arrows denote

944   colocalization; white outlined arrows denote lack of colocalization. Scale bars: 20 μm (main

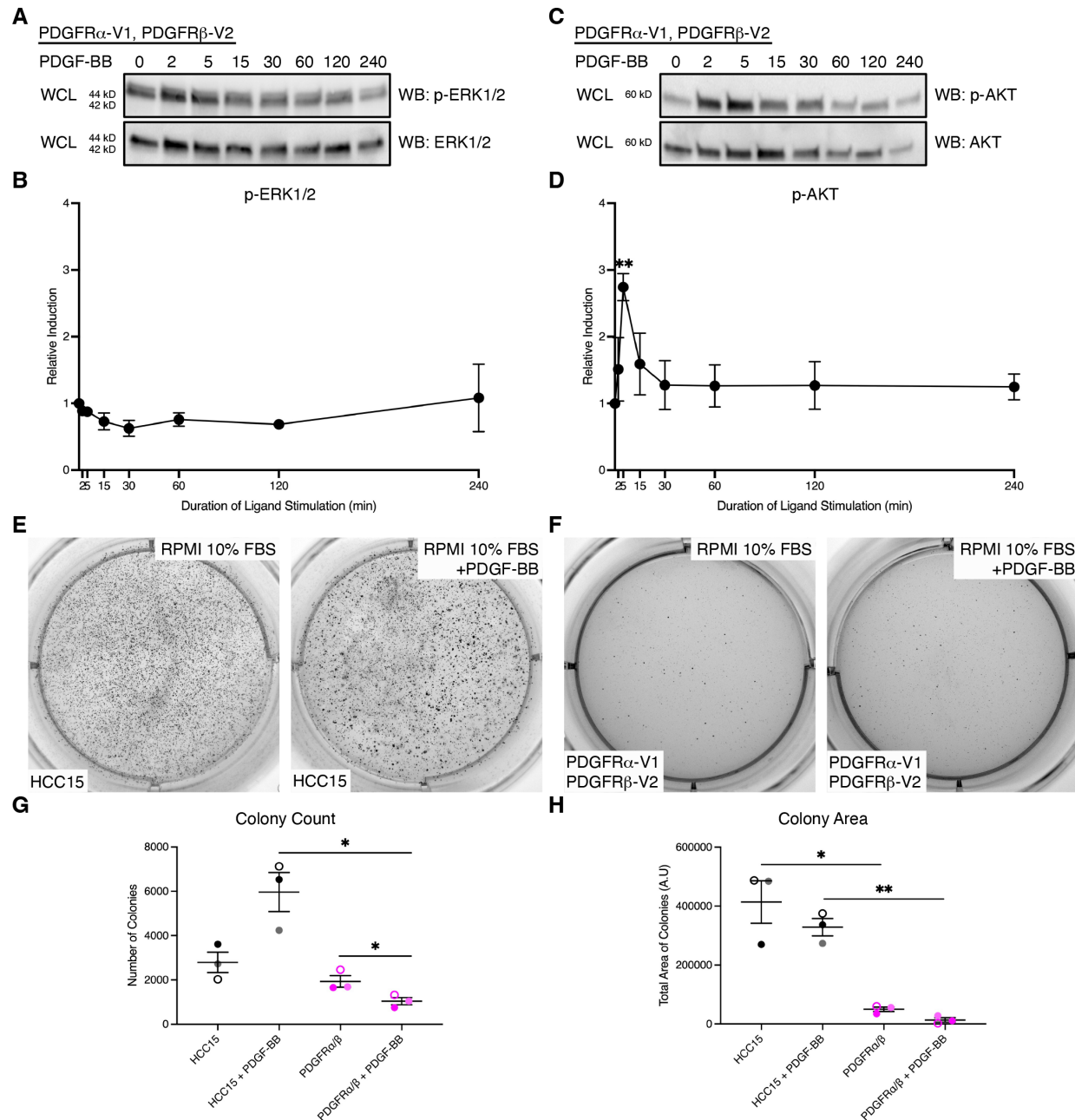945   images), 3 μm (insets).

946

45

947

Fig. 4. PDGFRα/β heterodimer activation does not induce downstream phosphorylation of

ERK1/2 and inhibits cell proliferation. (A,C) Western blot (WB) analysis of whole-cell lysates

(WCL) from the PDGFRα/β heterodimer cell line following a time course of PDGF ligand

stimulation from 2 min to 4 h with anti-phospho (p)-ERK1/2 (A) or anti-phospho (p)-AKT (C)

antibodies. **(B,D)** Line graphs depicting quantification of band intensities from *n*=3 biological

46

953   replicates as in A and C. Data are mean±s.e.m. **P<0.01 (two-tailed, ratio paired t-test). (**E,F**)

954   Colony growth in soft agar anchorage-independent growth assays for the HCC15 cell line (E) or

955   the PDGFRα/β heterodimer cell line (F) after 10 days in RPMI growth medium in the absence or

956   presence of PDGF-BB ligand in six-well plate wells. (**G,H**) Scatter dot plots depicting

957   quantification of colony count (G) or colony area (H) from n=3 biological replicates as in E and

958   F. Data are mean±s.e.m. *P<0.05; **P<0.01 (two-tailed, paired t-test within each cell line and a

959   two-tailed, unpaired t-test with Welch's correction between each cell line). Colored symbols

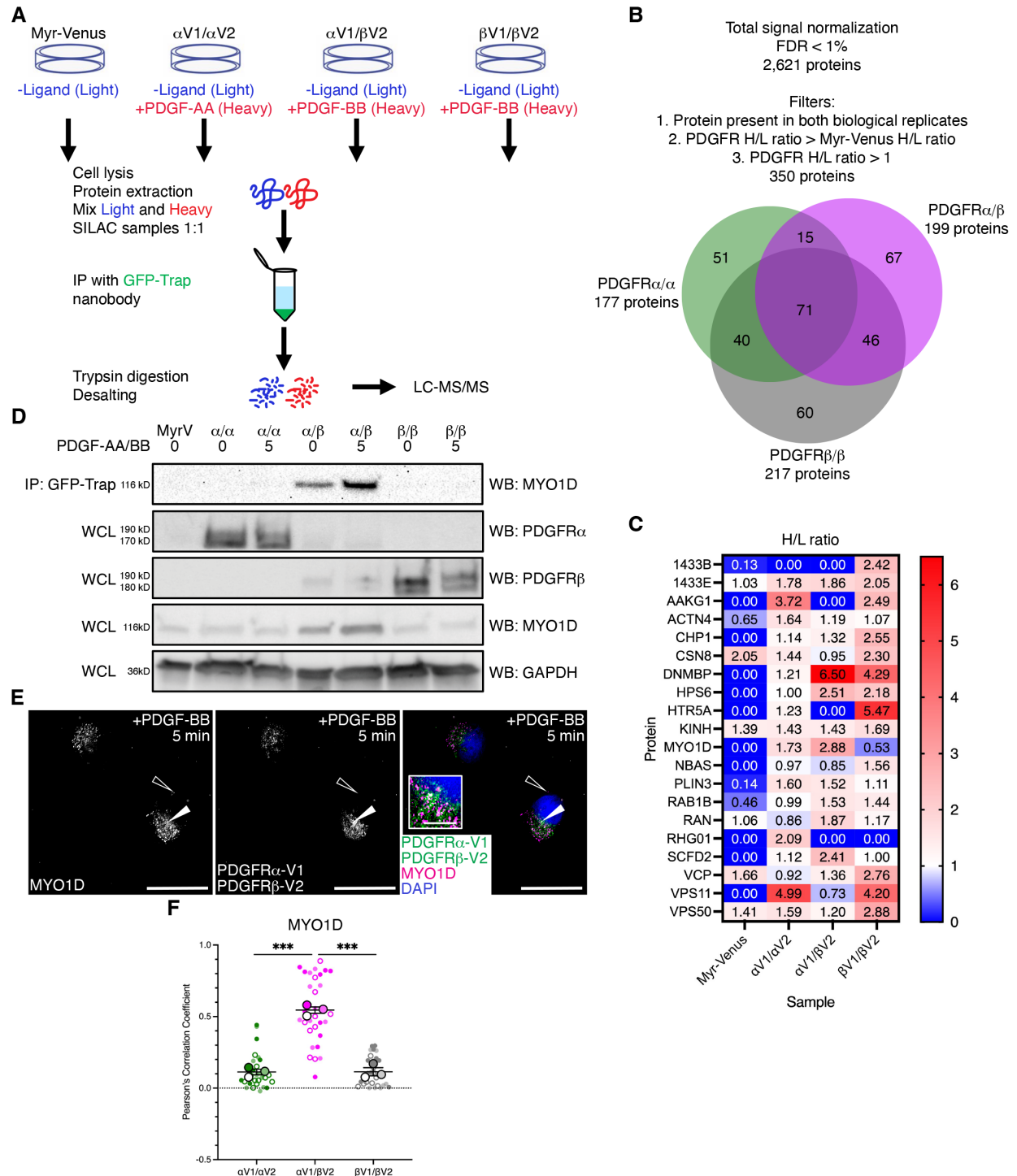960   correspond to independent experiments.

961

47

Fig. 5. MYO1D preferentially binds PDGFRα/β heterodimers. (A) Schematic depicting

experimental workflow for identification of PDGFR dimer-specific interacting proteins. **(B)**

Filters applied to the mass spectrometry data set and Venn diagram displaying shared protein

966   identifications between samples within the filtered data. (**C**) Heat map of heavy (H)/light (L)

967   SILAC ratios for identified proteins involved in trafficking. (**D**) Immunoprecipitation (IP) of

968   myristoylated Venus and dimerized PDGFR receptors with GFP-Trap nanobody from cells that

969   were unstimulated or treated with PDGF ligand for 5 min followed by western blotting (WB)

970   with an anti-MYO1D antibody. WCL, whole-cell lysates. (**E**) MYO1D antibody signal (white or

971   magenta) and/or Venus expression (white or green) as assessed by (immuno)fluorescence

972   analysis of the PDGFRα/β heterodimer cell line following PDGF-BB ligand stimulation for 5

973   min. Inset in E is a region where white arrows are pointing. Nuclei were stained with DAPI

974   (blue). White arrows denote colocalization; white outlined arrows denote lack of colocalization.

975   Scale bars: 20 µm (main images), 3 µm (insets). (**F**) Scatter dot plot depicting Pearson's

976   correlation coefficient of the PDGFRα homodimer, PDGFRα/β heterodimer or PDGFRβ

977   homodimer cell line Venus signal with an anti-MYO1D antibody signal following PDGF ligand

978   stimulation for 5 min as in E. Data are mean±s.e.m. ***$P<0.001$ (two-tailed, unpaired t-test with

979   Welch's correction). Colored circles correspond to independent experiments. Summary statistics

980   from biological replicates consisting of independent experiments (large circles) are superimposed

981   on top of data from all cells; n=10 technical replicates across each of three biological replicates.
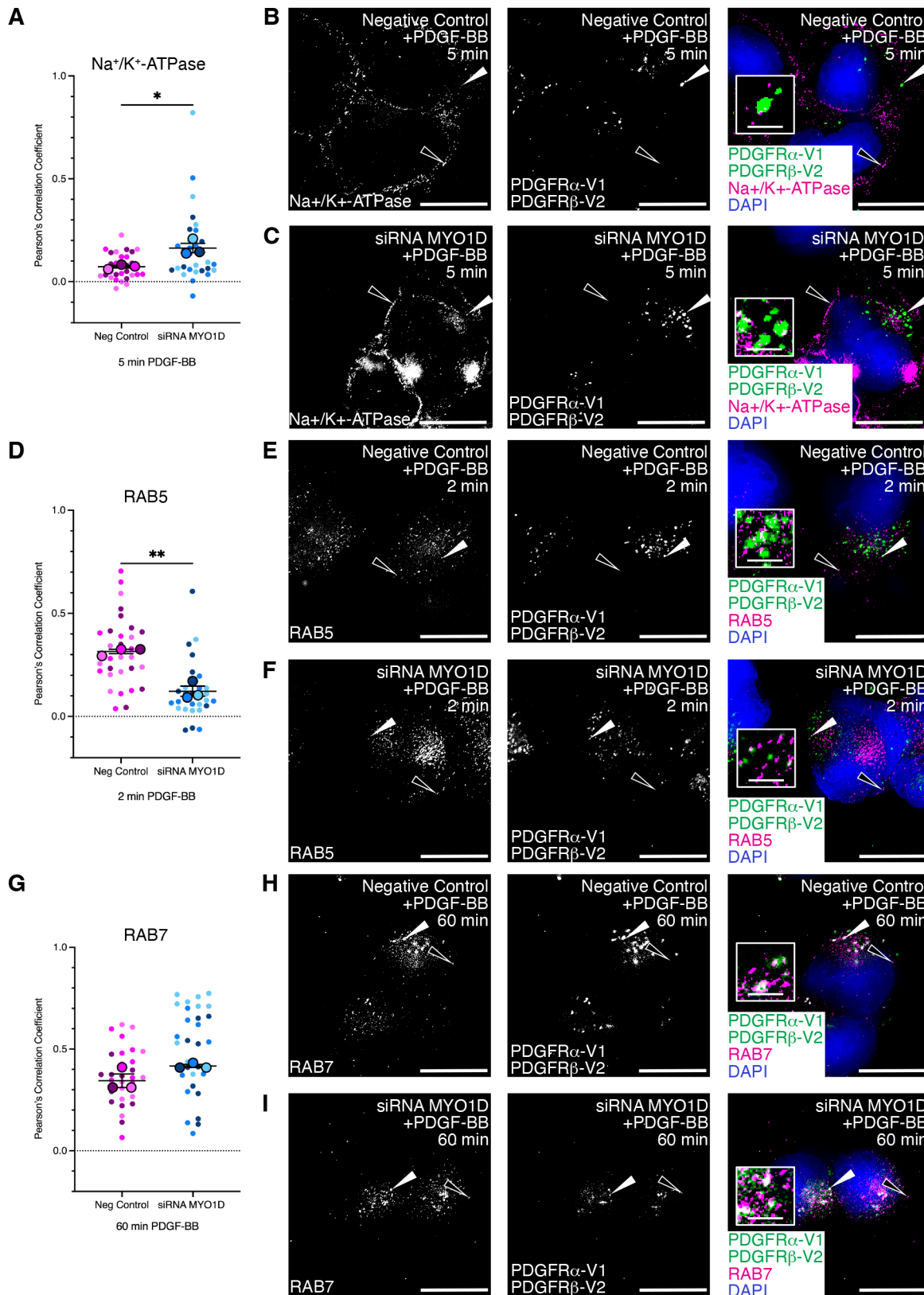
982

983

50

984 **Fig. 6. Knockdown of MYO1D leads to retention of PDGFRα/β heterodimers at the plasma**

985 **membrane.** (**A,D,G**) Scatter dot plots depicting Pearson's correlation coefficient of Venus signal

986 from the PDGFRα/β heterodimer cell line treated with Silencer Select negative control or

987 Silencer Select siRNA against MYO1D with an anti-Na$^+$/K$^+$-ATPase antibody (A), an anti-RAB5

988 antibody (D) or an anti-RAB7 antibody (G) signal following PDGF-BB ligand stimulation for 5

989 min (A), 2 min (D) or 60 min (G). Data are mean±s.e.m. *P<0.05; **P<0.01 (two-tailed,

990 unpaired *t*-test with Welch's correction). Colored circles correspond to independent experiments.

991 Summary statistics from biological replicates consisting of independent experiments (large

992 circles) are superimposed on top of data from all cells; *n*=10 technical replicates across each of

993 three biological replicates. (**B,C,E,F,H,I**) Na$^+$/K$^+$-ATPase antibody signal (white or magenta;

994 B,C), RAB5 antibody signal (white or magenta; E,F) or APPL1 antibody signal (white or

995 magenta; H,I) and/or Venus expression (white or green; B,C,E,F,H,I) as assessed by

996 (immuno)fluorescence analysis of the PDGFRα/β heterodimer cell line. Insets in B, C, E, F, H

997 and I are regions where white arrows are pointing. Nuclei were stained with DAPI (blue;

998 B,C,E,F,H,I). White arrows denote colocalization; white outlined arrows denote lack of

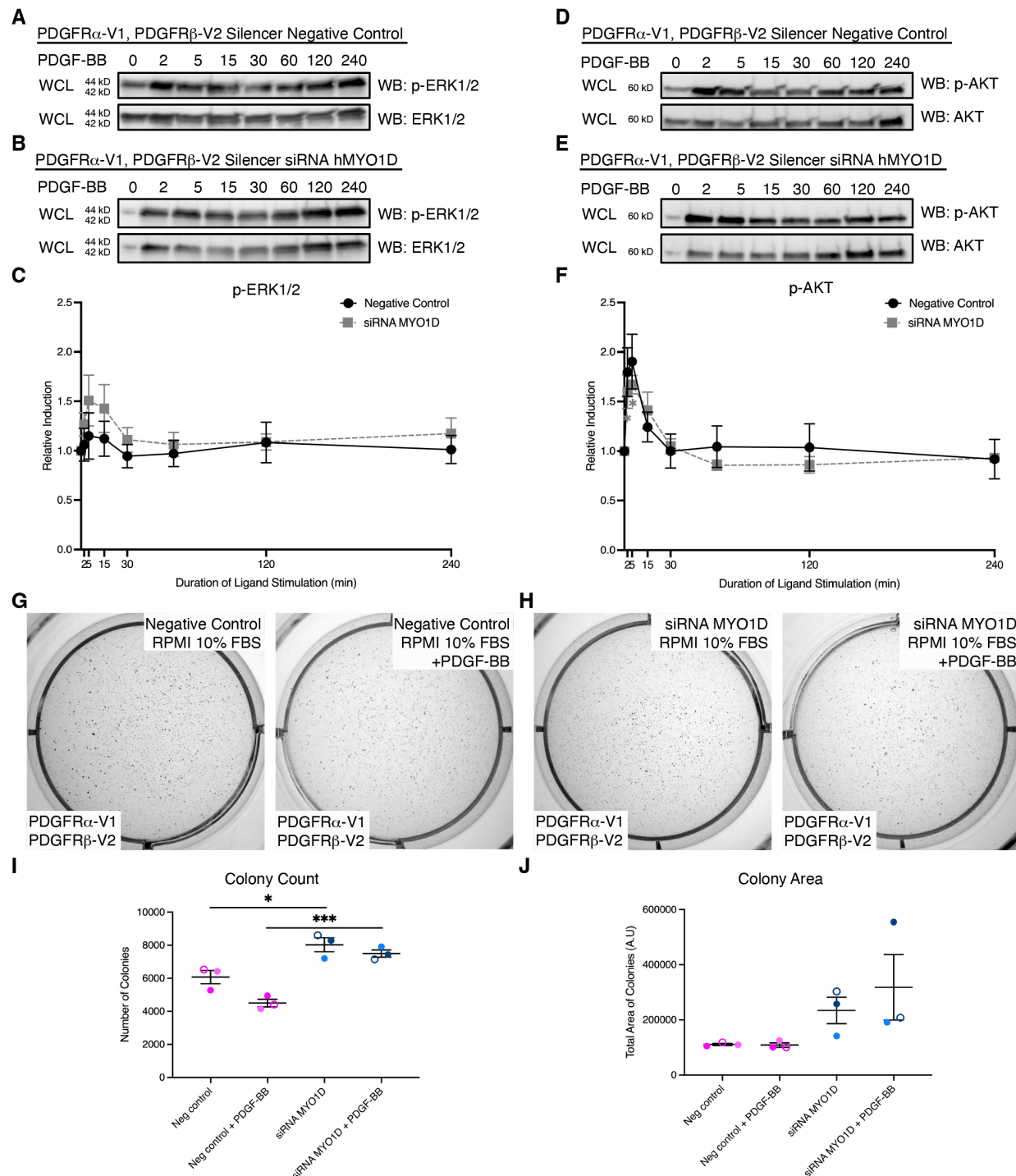999 colocalization. Scale bars: 20 µm (main images), 3 µm (insets).

1000

Fig. 7. Knockdown of MYO1D leads to increased downstream phosphorylation of ERK1/2 and increased cell proliferation. (A,B,D,E) Western blot (WB) analysis of whole-cell lysates (WCL) from the PDGFRα/β heterodimer cell line treated with Silencer Select negative control

1005   (A,D) or Silencer Select siRNA against MYO1D (B,E) following a time course of PDGF-BB

1006   ligand stimulation from 2 min to 4 h with anti-phospho (p)-ERK1/2 (A,B) or anti-phospho (p)-

1007   AKT (D,E) antibodies. (**C,F**) Line graphs depicting quantification of band intensities from $n=3$

1008   biological replicates as in A, B, D and E. Data are mean±s.e.m. *$P<0.05$ (two-tailed, ratio

1009   paired t-test). (**G,H**) Colony growth in soft agar anchorage-independent growth assays for the

1010   PDGFRα/β heterodimer cell line treated with Silencer Select negative control (G) or Silencer

1011   Select siRNA against MYO1D (H) after 10 days in RPMI growth medium in the absence or

1012   presence of PDGF-BB ligand in six-well plate wells. (**I,J**) Scatter dot plots depicting

1013   quantification of colony count (I) or colony area (J) from $n=3$ biological replicates as in G and H.

1014   Data are mean±s.e.m. *$P<0.05$; ***$P<0.001$ (two-tailed, paired t-test within each siRNA

1015   treatment and a two-tailed, unpaired t-test with Welch's correction between each siRNA

1016   treatment). Colored symbols correspond to independent experiments.